atmosphere

MDPI

Article

Air Temperature Extremes in the Mediterranean Region (1940–2024): Synoptic Patterns and Trends

Georgios Kotsias [1,*] and Christos J. Lolis [2]

[1] Eratosthenes Centre of Excellence, Limassol 3012, Cyprus
[2] Laboratory of Meteorology & Climatology, Department of Physics, University of Ioannina, 45110 Ioannina, Greece; chlolis@uoi.gr
* Correspondence: george.kotsias@eratosthenes.org.cy

Abstract

Extreme air temperatures along with the synoptic conditions leading to their appearance are examined for the Mediterranean region for the 85-year period of 1940–2024. The data used are daily (04UTC and 12UTC) grid point (1° × 1°) values of 2 m air temperature, 850 hPa air temperature, and 1000 hPa and 500 hPa geopotential heights, obtained from the ERA5 database. For 12UTC and 04UTC, the 2 m air temperature anomalies are calculated and are used for the definition of Extremely High Temperature Days (EHTDs) and Extremely Low Temperature Days (ELTDs), respectively. Overall, 3787 EHTDs and 4872 ELTDs are defined. It is found that EHTDs are evidently more frequent in recent years (increased by 305% since the 1980s) whereas ELTDs are less frequent (decreased by 41% since the 1980s), providing a clear sign of warming of the Mediterranean climate. A multivariate statistical analysis combining factor analysis and k-means clustering, known as spectral clustering, is applied to the data resulting in the definition of nine EHTD and seven ELTD clusters. EHTDs are mainly associated with intense solar heating, blocking anticyclones and warm air advection. ELTDs are connected to intense radiative cooling of the Earth's surface, cold air advection and Arctic outbreaks. This is a unique study for the Mediterranean region utilizing the high-resolution ERA5 data collected since the 1940s to define and investigate the variability of both high and low temperature extremes using a validated methodology.

Keywords: extreme air temperatures; Mediterranean region; synoptic patterns; spectral clustering; ERA5; climate change

Academic Editor: Hua Lu

Received: 30 May 2025
Revised: 7 July 2025
Accepted: 10 July 2025
Published: 13 July 2025

Citation: Kotsias, G.; Lolis, C.J. Air Temperature Extremes in the Mediterranean Region (1940–2024): Synoptic Patterns and Trends. *Atmosphere* **2025**, *16*, 852. https://doi.org/10.3390/atmos16070852

1. Introduction

Climate change is one of the most vital challenges of the 21st century affecting our everyday lives and shaping our future. Temperatures are rising on a global scale affecting human health and agriculture and threatening entire ecosystems. These temperature increases are the result of the continuous human intervention in the natural greenhouse effect, mainly by activities such as fossil fuel combustion and deforestation [1]. Extreme temperatures are associated with significant energy exchanges between the surface and the atmosphere, contributing to the development of intense weather events such as heatwaves and droughts [2,3]. These extreme temperature events are associated with increased heat-related mortality, particularly among vulnerable and urban populations. Furthermore, the Mediterranean's economic sector heavily depends on agriculture and tourism, and the increasing frequency and intensity of temperature extremes have a negative impact by undermining agricultural productivity, disrupting seasonal cycles and affecting water

resources. Therefore, studying those temperature extremes and the synoptic conditions favoring their occurrence are of critical importance for understanding their characteristics and mitigating their impact on our planet.

The Mediterranean region is an area actively experiencing the results of ongoing climate change [1,4,5] and is occasionally referred to as a "climate change hotspot" [6]. Multiple studies over the past decades focused on the Mediterranean temperature variability have documented a general warming trend, particularly pronounced in the spring and autumn seasons, with the highest temperatures recorded in recent decades. While western Mediterranean areas consistently show increasing extreme summer temperatures, eastern parts have exhibited a more complex behavior, with periods of "cooling" that have reversed in the last two decades [7–9]. Climate projection models and reanalysis data further reveal distinct regional contrasts, with southern Mediterranean areas facing more intense temperature extremes and notable shifts in precipitation patterns [10–14]. Specifically, the eastern Mediterranean and Middle East regions are warming nearly twice as fast as the global average, with future projection scenarios indicating the increasing frequency, duration and intensity of heatwaves under high emission scenarios [12,15,16]. These findings highlight the importance and urgency of understanding temperature extremes and the associated atmospheric conditions leading to their appearance across the Mediterranean basin to better anticipate their occurrence, improve early warning systems and mitigate future climate impacts.

In the present study, the high spatiotemporal resolution ERA5 reanalysis data are utilized for the study of temperature extremes in the Mediterranean region. Relevant research studies follow an objective or subjective approach by establishing thresholds for defining temperature extremes. The objective approach is based on statistical parameters, whereas the subjective approach is focused on the researcher's climatological experience. In this study, temperature extremes are defined following an objective approach, and their relationship to synoptic atmospheric patterns is investigated using a multivariate statistical technique. The methodology applied here is similar to the approach followed by Lolis et al. [11] for the Balkans region. In Section 2, the data used and the applied methodology are analyzed in detail.

The novelty of this work lies in the use of the high-resolution ERA5 dataset to objectively define both high and low temperature extremes throughout the year and across the entire Mediterranean region for a large time period, by applying a validated multivariate statistical methodology. Additionally, by linking these extreme events with the synoptic-scale atmospheric circulation patterns, this study offers valuable insights into the underlying drivers of temperature extremes. As such, it makes a significant contribution to the understanding of the Mediterranean climate variability.

The aim of this work is to (1) define extremely high/low temperature days by using an objective multivariate methodology, (2) investigate the intra-annual and inter-annual variability of the extreme days along with statistically significant long-term trends, (3) classify into clusters/groups the extreme days with the synoptic patterns leading to their occurrence, (4) identify the seasonal and spatial variations in the defined clusters.

2. Materials and Methods

2.1. Data

The data used in this work are obtained from the fifth generation of atmospheric reanalysis (ERA5, [17]) instruments produced by the European Centre for Medium-Range Weather Forecasts (ECMWF) as part of the Copernicus Climate Change Service (C3S). ERA5 provides a variety of land, sea and atmospheric variables by combining model data with observations from satellites and in situ measurements and using advanced data assimilation

techniques (reanalysis). The data have a spatial resolution of up to 0.25° × 0.25°, an hourly temporal resolution and are dating back to 1940, so more than 80 years of data are available today. In the present work, the daily (at 04UTC and 12UTC) values of air temperature at 2 m above the Earth's surface (T), 850 hPa air temperature (T850) and 1000 hPa and 500 hPa geopotential heights (GH1000 and GH500) for the Mediterranean region (50° N–30° N, 10° W–40° E, Figure 1) are used. The data have a spatial resolution of 1° × 1° and refer to the period 1/1/1940–31/12/2024, so 85 years of data are used. The extremely high/low temperatures are determined by the values of T at 12 and 04 UTC, respectively, and the relationship between the defined temperature extremes and the characteristics of synoptic circulation patterns is examined using the T850, GH1000 and GH500 values. Although ERA5 provides data at a higher spatial resolution of 0.25° × 0.25°, a coarser 1° × 1° resolution was used in this work. This choice reflects the synoptic-scale focus of the study, aiming to identify spatially coherent extreme temperature events and their associated large-scale circulation patterns. Using a coarser resolution reduces regional 'noise' and small-scale variability, such as those introduced by microclimatic effects in mountainous or coastal regions, leading to a clearer determination of spatially coherent extreme events and synoptic-scale atmospheric patterns [7,8]. This approach enhances the robustness of the statistical analysis and is commonly adopted in climatic studies of large-scale extremes, as it preserves the main spatial patterns and long-term trends of meteorological variables while minimizing the influence of localized effects or station-level biases [12]. However, it must be noted that ERA5 data, like all reanalysis products, is subject to uncertainties, especially before the assimilation of satellite observations, potentially affecting the accuracy of temperature fields and atmospheric circulation patterns during that period [17].

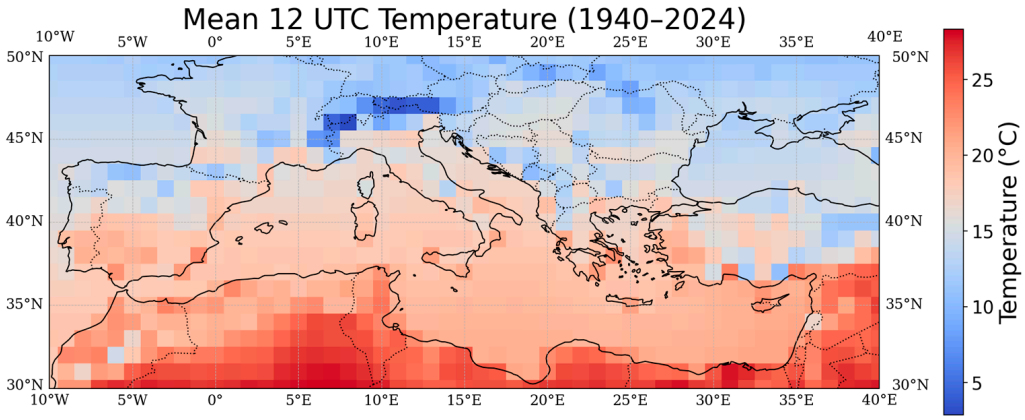

Figure 1. The long-term mean of 12 UTC 2 m air temperature (1940–2024) over the geographical domain of the greater Mediterranean region.

2.2. Methodology

For the definition of the temperature extremes, from the daily T values at 12:00 UTC the high temperature extremes are defined, whereas the T values at 04:00 UTC are used to determine the extremely low temperature cases. These two hours are selected considering the daily variation in air temperature and the time of occurrence of daily maximum and minimum temperatures. In the next step, a procedure for the definition of a day as an extreme is followed. The long-term mean values of T, as well as the standard deviations, for the period 1940–2024 are computed for each of the 365 dates in the year (1/1–31/12) at each grid point of the domain (Figure 1). In order to reduce the noise in the mean daily intra-annual variations in T, a 5-day moving average smoothing procedure is followed. The use of a 5-day moving average allows for a more robust identification of sustained extreme temperature events by reducing the influence of short-term fluctuations. This approach is appropriate for investigating synoptic-scale anomalies and has been commonly adopted

in similar studies [11,18]. As a result, each daily T value (T_d) is replaced by the average value of the 5 closest days (T_{d-2}, T_{d-1}, T_d, T_{d+1}, T_{d+2}). Then, the temperature anomaly (TA) values are calculated at each grid point and for each day of the year, by subtracting the corresponding 5-day moving averages from the T values. By using TA values, the influence of the strong seasonal cycle is ignored, allowing the detection of high and low temperature extremes throughout the whole year. Also, it should be noted that the use of a constant threshold of T as the indicator for the definition of temperature extremes is not appropriate for the present study, because temperature in the Mediterranean region presents a strong latitudinal gradient and strong seasonal variability. Thus, such a selection would confine high temperature extremes in summer—particularly in the southern areas—and low temperature extremes in winter—particularly in the northern areas. The characterization of a temperature value as extreme has to be made considering its deviation from the long-term mean (normal) value for the specific area and the specific season of the year, because, in this way, abnormal conditions of various causes and consequences are identified and studied in the whole region during the whole year. This provides analytical evidence regarding the climate variability in the region. Next, a spatial threshold indicator is applied. If at least 5% of the grid points (54/1071) have a TA more than two standard deviations from the corresponding 5-day moving average long-term mean, the day is classified as an Extremely High Temperature Day (EHTD). Similarly, if at least 5% of the grid points (54/1071) have a TA less than two standard deviations from the corresponding 5-day moving average long-term mean, the day is classified as an Extremely Low Temperature Day (ELTD). The spatial coverage threshold is used in order to eliminate spatially isolated instances of extremes, which are most likely related to regional micrometeorological causes [11]. The method was also attempted using spatial coverage thresholds of 1% and 10% but the resulting number of defined extreme cases were either too many (>12000) or too few (<2000) in regards to the size of the dataset. Consequently, we adopted the 5% spatial coverage threshold as the most balanced indicator and the most commonly used in relevant studies [11]. Since the definition of temperature extremes is based on the deviations of T from the normal values of the corresponding dates of the year (anomalies), rather than constant thresholds of T, it is guaranteed that they are detected throughout the year and not just during the warm (for EHTDs) and cold (for ELTDs) periods of the year. Furthermore, the temperature anomaly ratio (TAR) is calculated by dividing the TA values by the respective standard deviation. The TAR is used to normalize anomalies across locations with diverse climate variability, allowing comparison between different regions.

Having defined the extreme temperature days, a statistical analysis is applied to investigate the connection between the temperature extremes and the synoptic atmospheric circulation patterns leading to their appearance. To accomplish this, a process known as "spectral clustering" [19,20] is applied, which includes the use of factor analysis (FA) followed by k-means cluster analysis (CA).

FA [21] is a multivariate statistical method that is frequently applied in climatological studies as a dimensionality reduction technique with the lowest possible loss of the initial data's total variance. It is a variant of Principal Component Analysis (PCA), but it specifically seeks to uncover latent variables (factors) that can explain the observed correlations among variables. In FA, a new set of m variables are created, called factors, which are much smaller in number compared with the initial set of n variables ($m << n$). Each initial variable is linearly correlated with one or more factors through correlation coefficients known as factor loadings. Basically, these loadings indicate how strongly each variable is associated with any factor, with higher values indicating strong correlation and representation. Rotation of the axes is a commonly used technique when applying FA and is used for maximizing the variance of the new variables and improving the physical interpretation

of the results [22]. In this work, varimax rotation is followed [23], which is an orthogonal rotation method widely used to improve the interpretability of the extracted factors. It works by maximizing the variance of the squared loadings within each factor. This results in a clearer separation of variables across factors, where each variable tends to correlate strongly with a single factor and weakly with others. Applying varimax rotation assists in producing a more distinct and interpretable grouping of variables, without compromising the explained variance.

CA [24] is a classification technique used for the categorization of variables into distinct and homogeneous groups, called clusters, according to a certain statistical parameter. In the present work, the Euclidean distance is used to quantify the similarity between variables. Based on this classification indicator, each variable is assigned to the cluster whose centroid it is nearest to, ensuring that variables within the same cluster are more similar to each other than to those in other clusters. In the k-means algorithm, CA runs multiple times for different number of clusters succeeding in the continuous rearrangement of the cases in new clusters [25]. The number of iterations used in k-means clustering algorithm was 47 and 52 for EHTDs and ELTDs, respectively. Then, a statistical test is applied, indicating the optimal number of clusters leading to the best possible classification of the parameters involved. In the present work, the distortion statistical test is followed for the selection of the number of clusters [26]. According to this method, a parameter called "jump" is calculated for each possible number of clusters. In the corresponding plot, the optimal number of clusters is the point where the jump sharply decreases ("elbow" point), beyond which adding more clusters does not significantly improve the quality of the grouping of the variables. However, to qualitatively test the robustness and sensitivity of clusters, various numbers of clusters slightly higher or lower than the optimum number indicated by the distortion test were used. By comparing the results, it was realized that the number of clusters indicated by the distortion test led to more distinct clusters with clear physical hypostasis.

In the present study, FA is applied to extract the dominant modes of variability by uncovering the underlying patterns in how different meteorological parameters covariate, allowing for a more physically interpretable dimensionality reduction compared with traditional Principal Component Analysis or Empirical Orthogonal Function approaches. Following with the application of CA on the FA defined factors' scores enables the objective classification of extreme temperature events into distinct groups with common synoptic characteristics, providing a more robust way for understanding their driving mechanisms. To investigate the existence of statistically significant trends, the Mann–Kendall test [27] at a 95% confidence level has been followed.

For each case of extreme temperature dates (EHTDs and ELTDs) two data matrices are constructed containing the TAR values and the atmospheric circulation parameters' values (GH1000, GH500 and T850). FA is applied to each matrix separately, in order to reduce the dimensionality, and the resulting factor scores' time series are stored in a unified matrix. CA is applied to the unified matrix, classifying the extreme temperature dates and the atmospheric circulation characteristics leading to their predominance, into distinct and homogenous clusters. Figure 2 shows the step-by-step methodology used in this study, including the application of FA and CA, leading to the definition of EHTD/ELTD clusters.

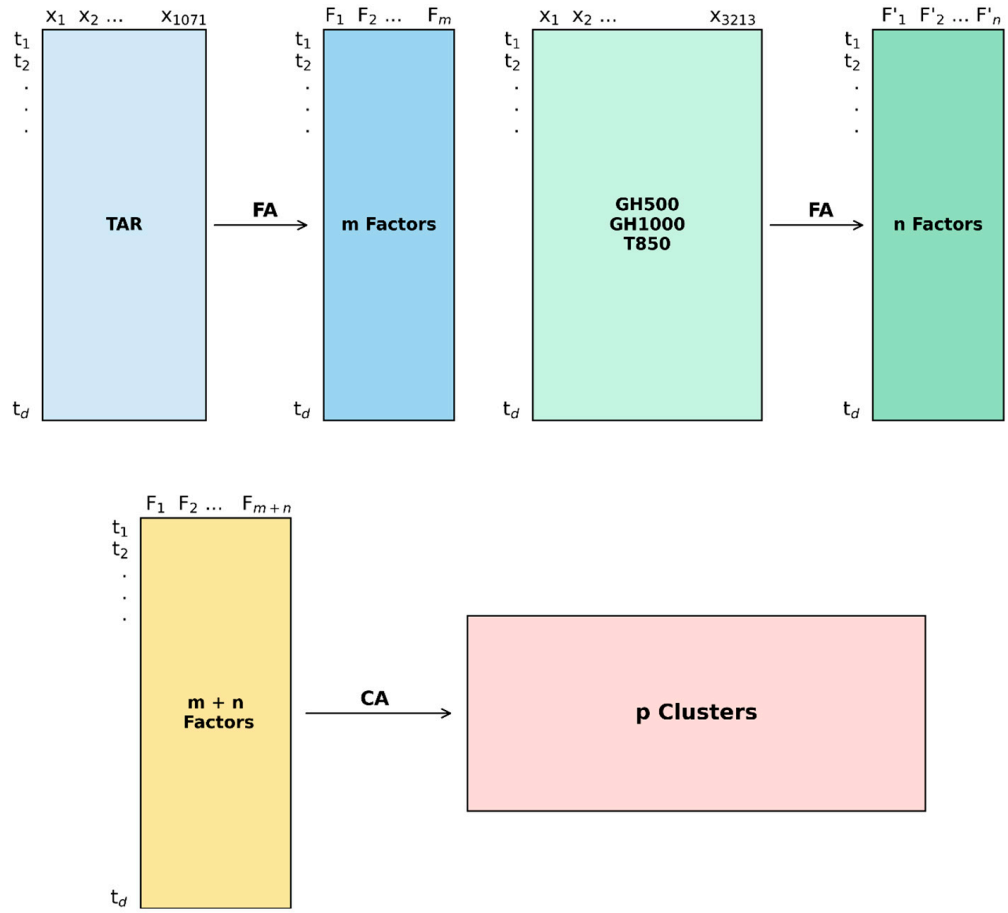

Figure 2. Schematic representation of the applied methodology.

3. Results and Discussion

3.1. Temperature Statistics

The long-term mean of 2 m air temperature at 12 UTC over the Mediterranean region for the period 1940–2024 is shown in Figure 1. The highest mean temperature values are observed across the southern and eastern parts of the domain, particularly over North Africa, Greece, Cyprus and the Middle East. On the contrary, the lowest mean temperature values are found over continental Europe, being most pronounced over central and eastern Europe, with a notable minimum over the Alpine region north of Italy. Figure 3 shows the mean temperature variability at 12 and 04 UTC across the Mediterranean. Figure 3a,b present the intra-annual and inter-annual variability, respectively, highlighting the strong seasonal cycle and year-to-year fluctuations in mean temperature. The mean annual temperatures at 12 UTC and 04 UTC fluctuate around 17 °C and 12 °C, respectively, until the early 2000s, after which a clear warming tendency becomes evident. Positive statistically significant trends are revealed (95% confidence level) in the inter-annual variability of both 12 and 04 UTC mean temperatures. These are clear indicators of the warming of the Mediterranean region, which has intensified during the last decade. Figure 3c,d compare the intra-annual temperature cycles between two distinct periods, 1940–1980 and 1981–2024, at 12 UTC and 04 UTC, respectively. It can be seen that the more recent period exhibits a consistent warming across all months, with the largest differences occurring during the early winter and early spring months. This finding also indicates a temperature increase in the Mediterranean during the most recent periods [28], likely reflecting the impact of the ongoing climate change in the region.

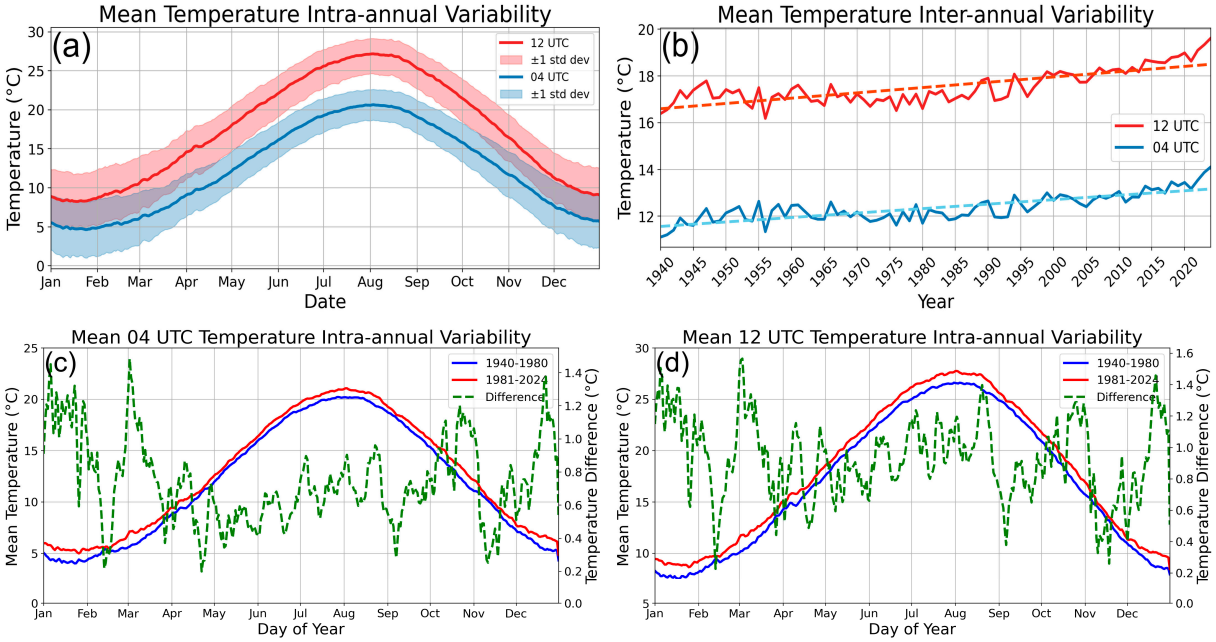

Figure 3. Mean temperature variability at 12 and 04 UTC: (**a**) intra-annual and (**b**) inter-annual variability; (**c**,**d**) intra-annual variability for 1940–1980 and 1981–2024 and their differences at (**c**) 12 UTC and (**d**) 04 UTC.

3.2. EHTDs

The application of the methodology described in Section 2.2 for the identification of EHTDs led to the definition of 3787 EHTDs. It is evident that these EHTDs are more frequent during the warm period of the year and the inter-annual variation in their number shows a statistically significant increase during the 85-year period of 1940–2024, meaning that EHTDs occurred more frequently in recent years, especially during the 21st century (Figure 4). The remarkable difference in the number of EHTDs between winter and summer is mainly due to differences between the two seasons concerning (i) the statistical distributions of the air temperature samples (different number of extreme high and extreme low values); (ii) the spatial extent of the extreme high temperature areas. In the inter-annual variations plot, the percentages and bar colors indicate the decadal-scale changes in the mean number of EHTDs compared with the previous decade. The green (or red) color of a decade denotes an increased (or decreased) mean number of EHTDs compared with the previous decade. The changes are shown as a percentage scale. Of course, the first decade, 1940–1949, does not have a previous decade to compare to and the last period, 2021–2024, is an incomplete decade, therefore they are shown in a gray color. The rapid increase in the mean number of EHTDs can easily be noticed with increasing percentages every passing decade. Comparing the mean number of defined EHTDs during the periods 1940–1980 and 1981–2024, an increase of 305% is found.

Applying FA to the TAR time series results in eight factors representing 74% of the total variance, whereas applying FA to the T850, GH1000 and GH500 time series yields five factors representing 82% of the total variance. In the next step, the 13 factor scores' time series are placed in a matrix and CA is applied, as shown in Figure 2. In Figure 5, the results of the distortion test applied to determine the optimal number of clusters for both Extremely High (EHTDs, Figure 5a) and Extremely Low Temperature Days (ELTDs, Figure 5b) are presented. As shown in Figure 5a for the EHTDs analysis, the test indicates that 9 or 11 clusters would be suitable choices. While both cases were tested, the 9 cluster classification was ultimately selected, as the 11 cluster classification case resulted in overlapping or highly similar clusters that could reasonably be merged.

Therefore, the classification of EHTDs along with their associated synoptic circulation patterns into nine distinct clusters is considered the most robust and interpretable solution for this analysis. Each cluster represents a physically meaningful grouping of EHTDs characterized by similar temperature anomaly distributions and the associated large-scale atmospheric circulation patterns. These patterns show the underlying synoptic conditions that consistently lead to extreme heat events across the Mediterranean region. For each cluster, the mean spatial patterns of TA, TAR, GH500, GH1000 and T850 are shown, along with the inter-monthly and inter-annual variations in the number of EHTDs (Figures 6–14).

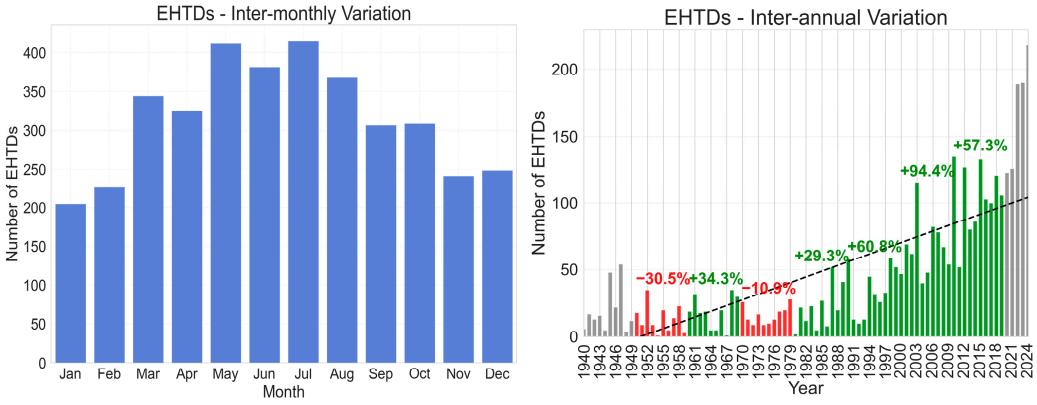

Figure 4. The inter-monthly (**left**) and the inter-annual (**right**) variations in the number of EHTDs. In the inter-annual plot, the percentages and bar colors indicate the decadal-scale changes in the mean number of EHTDs compared with the previous decade (green for an increase and red for a decrease). The gray bars represent the first decade, 1940–1949, and the incomplete decade, 2021–2024. The dashed line represents the statistically significant linear trend at 95% confidence level.

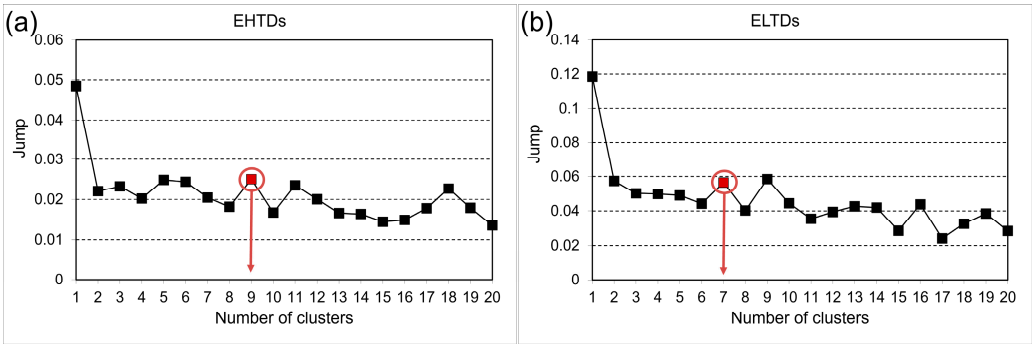

Figure 5. The results of the distortion test for the classification of (**a**) EHTDs and (**b**) ELTDs. The optimal number of clusters are indicated by the red circle.

CL1 (Figure 6) is generally a cold period cluster with the highest frequency of occurrence during the spring season (March to May). This type of EHTDs seems to be more frequent in recent years, as shown by the positive (statistically significant) trend in the inter-annual variation. The TA and TAR values are high over the western Mediterranean including the Iberian Peninsula and Algeria. The synoptic conditions leading to the appearance of such EHTDs, include the prevalence of anticyclonic conditions over NW Africa, a mid-tropospheric ridge and high T850 values. These high-pressure systems act as a heat dome, trapping the warm air, preventing cloud formation and causing prolonged heating. The observed increase in CL1 EHTDs aligned with the findings of Zhang et al. [29], who showed that intensifying heat domes under global warming increasingly contribute to temperature extremes during spring.

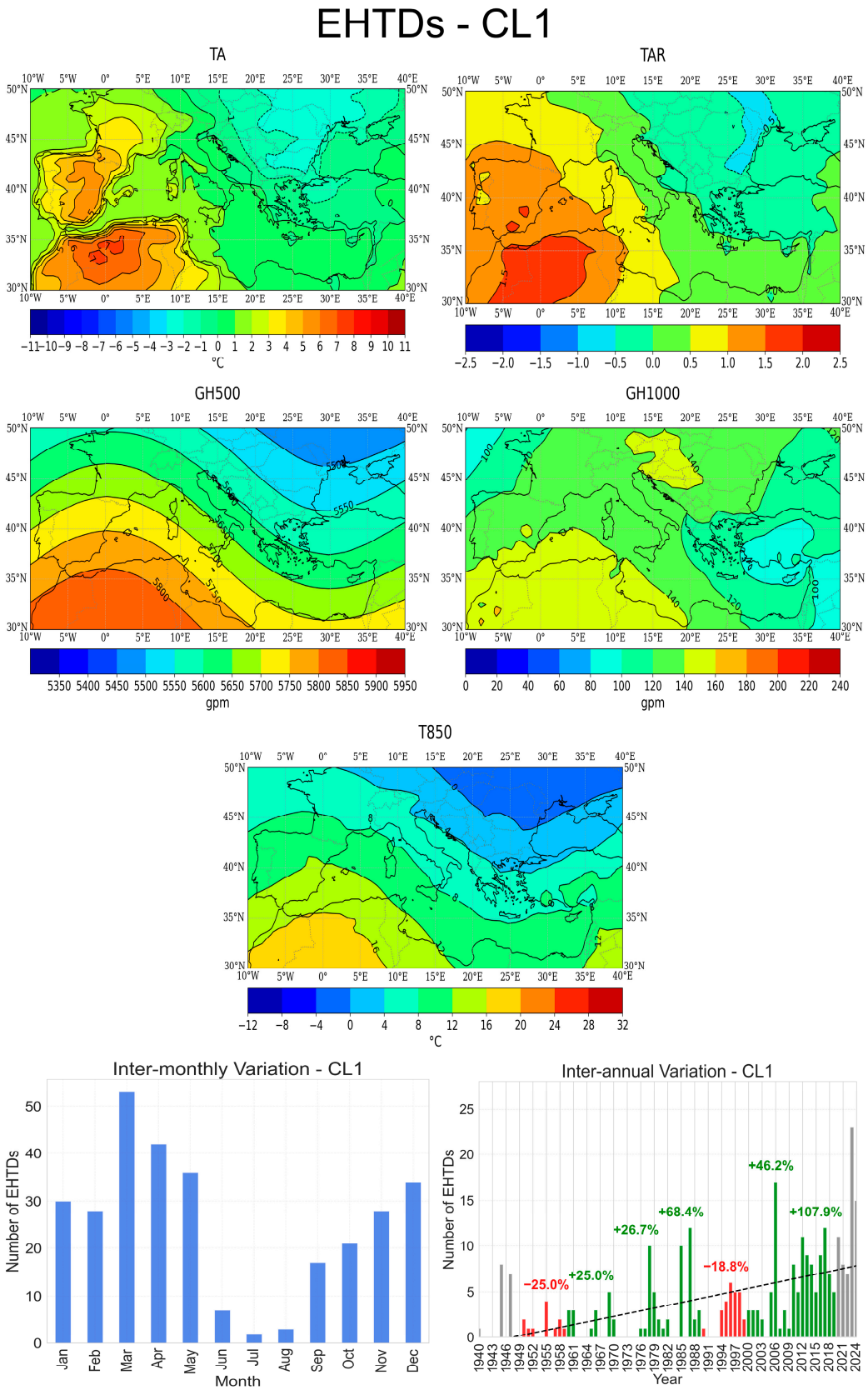

Figure 6. The TA (°C), TAR (unitless), GH500 (geopotential meters, gpm), GH1000 (geopotential meters, gpm) and T850 (°C) mean patterns and the respective inter-monthly and inter-annual variations for CL1 of EHTDs. Statistically significant trends in the inter-annual variation are shown (dashed line).

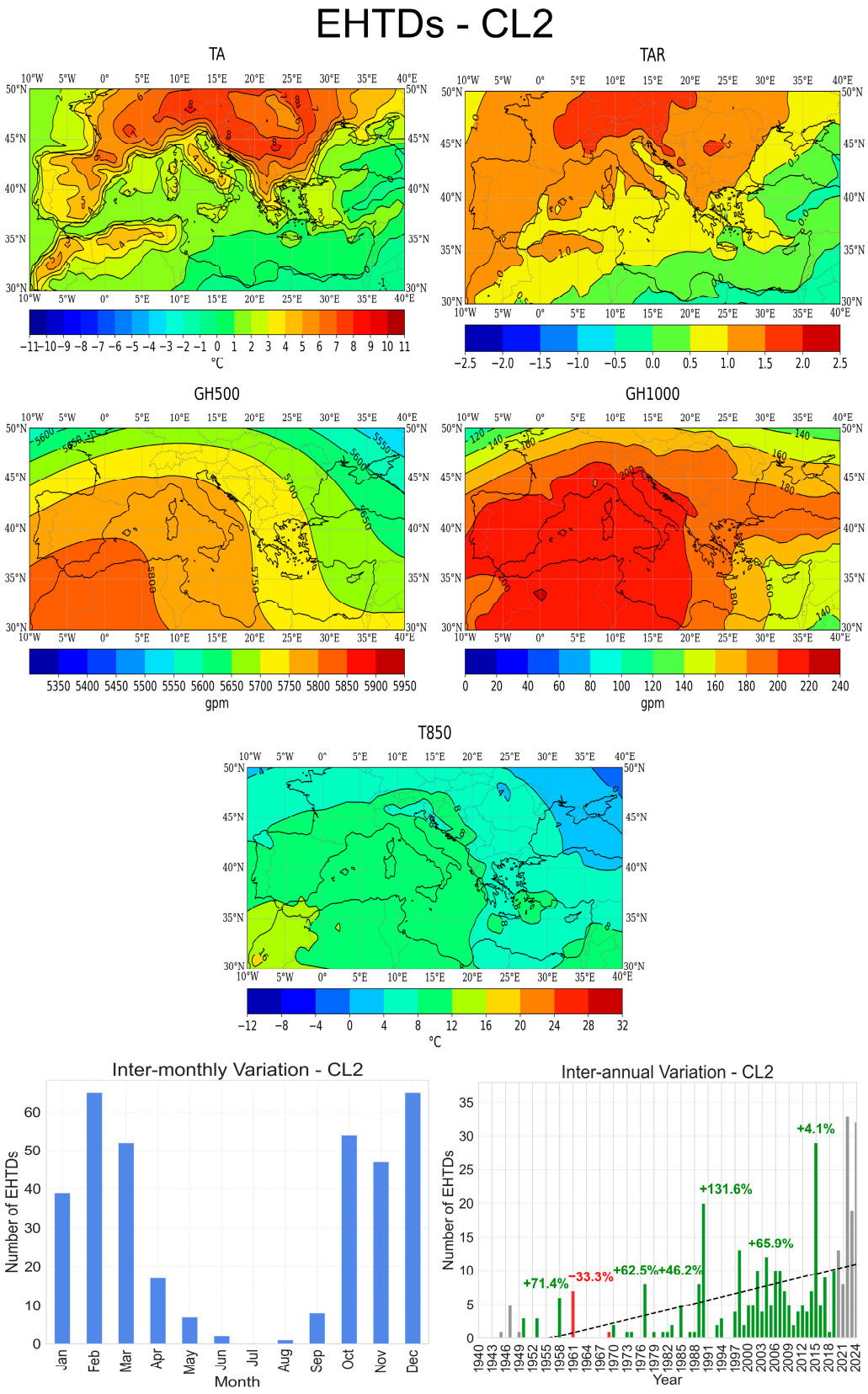

Figure 7. Same as in Figure 6, but for CL2 of EHTDs.

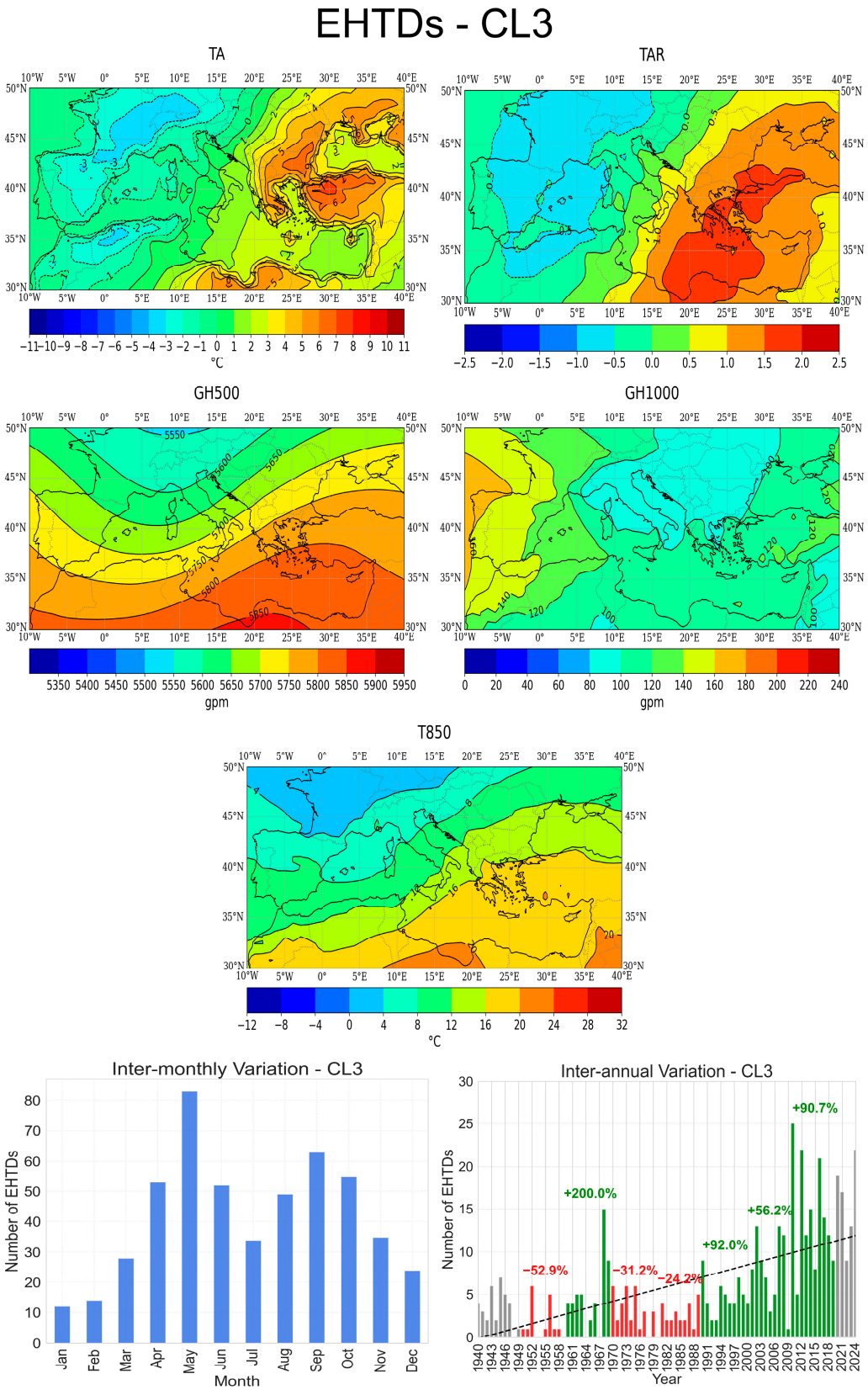

Figure 8. Same as in Figure 6, but for CL3 of EHTDs.

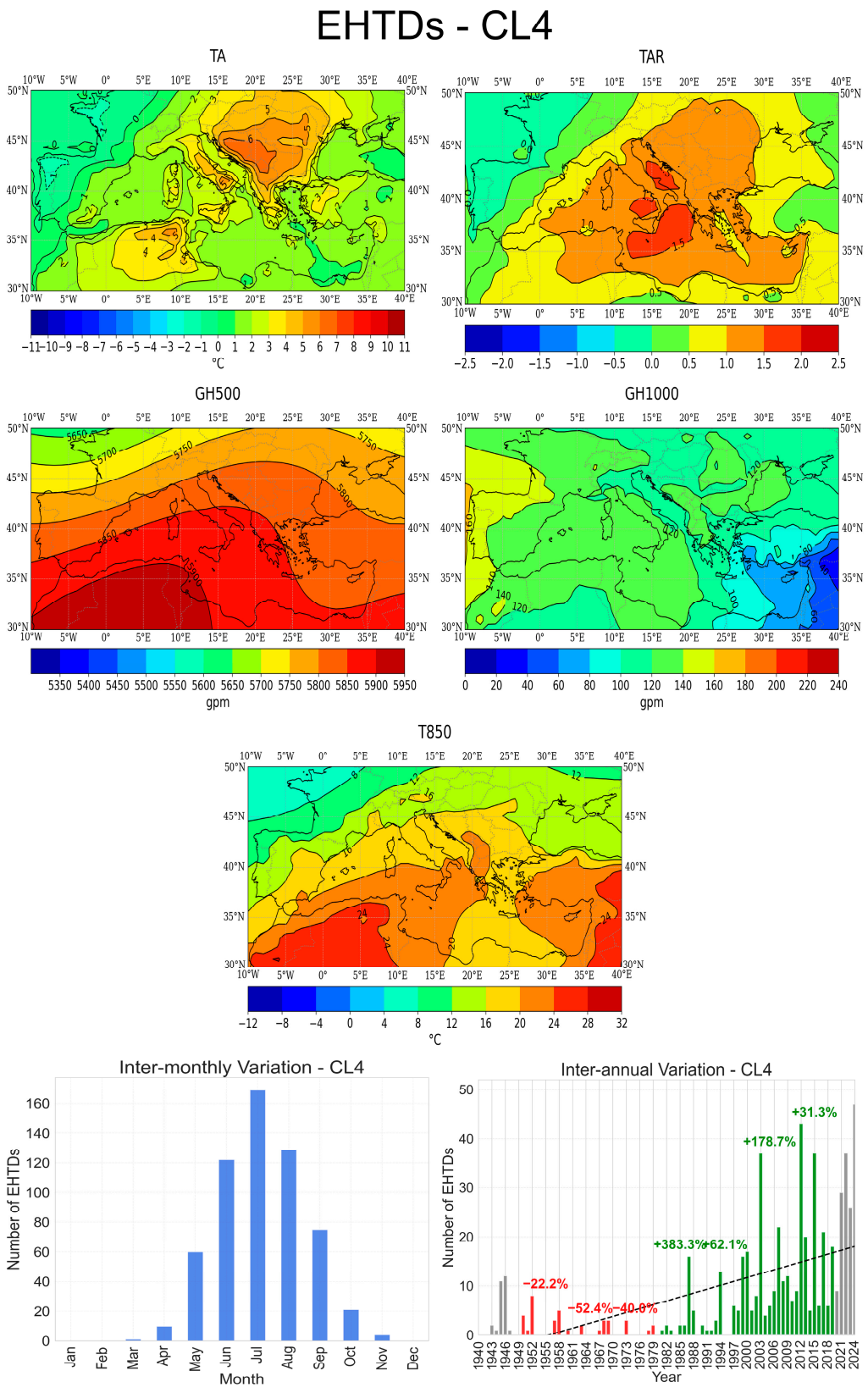

Figure 9. Same as in Figure 6, but for CL4 of EHTDs.

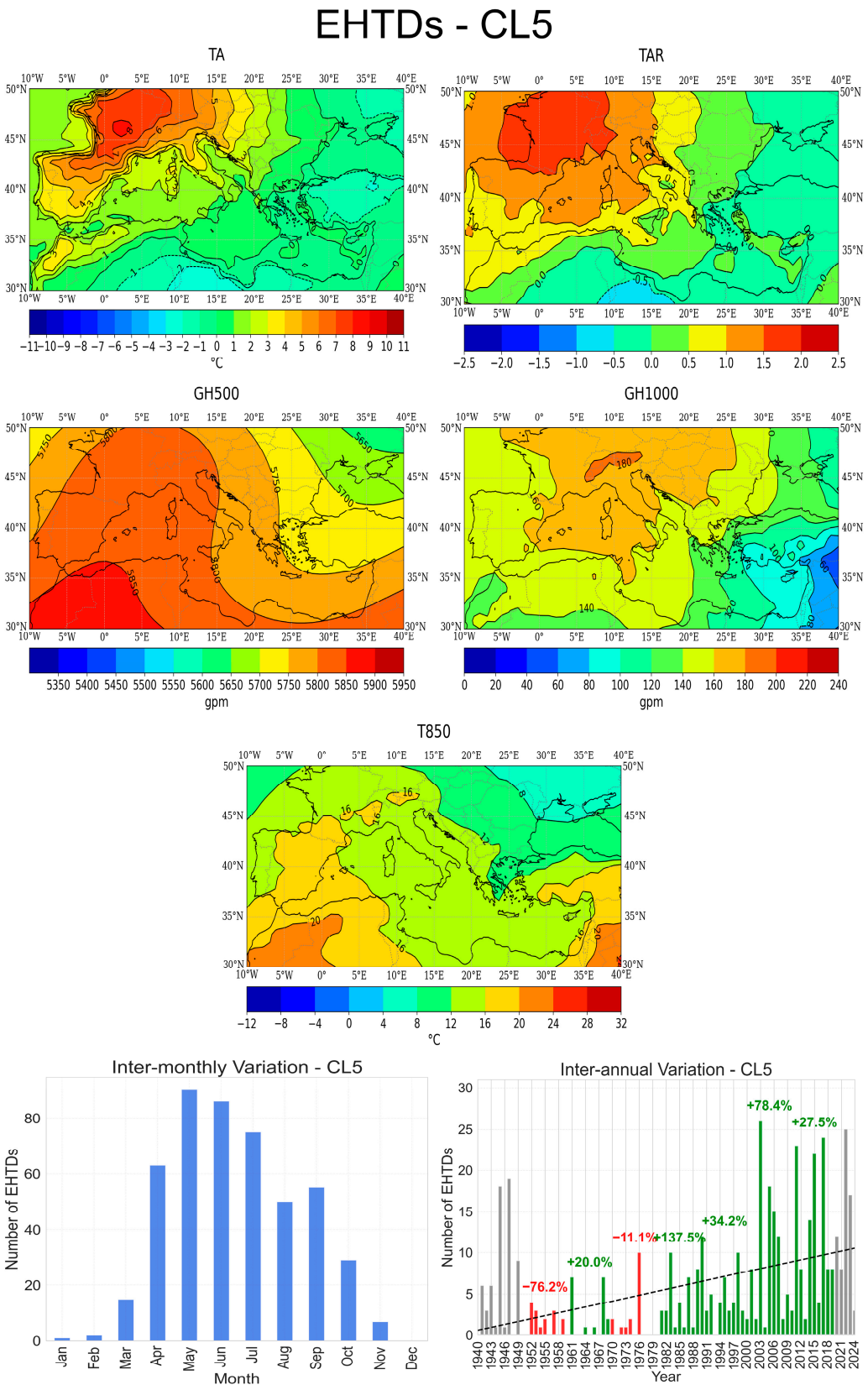

Figure 10. Same as in Figure 6, but for CL5 of EHTDs.

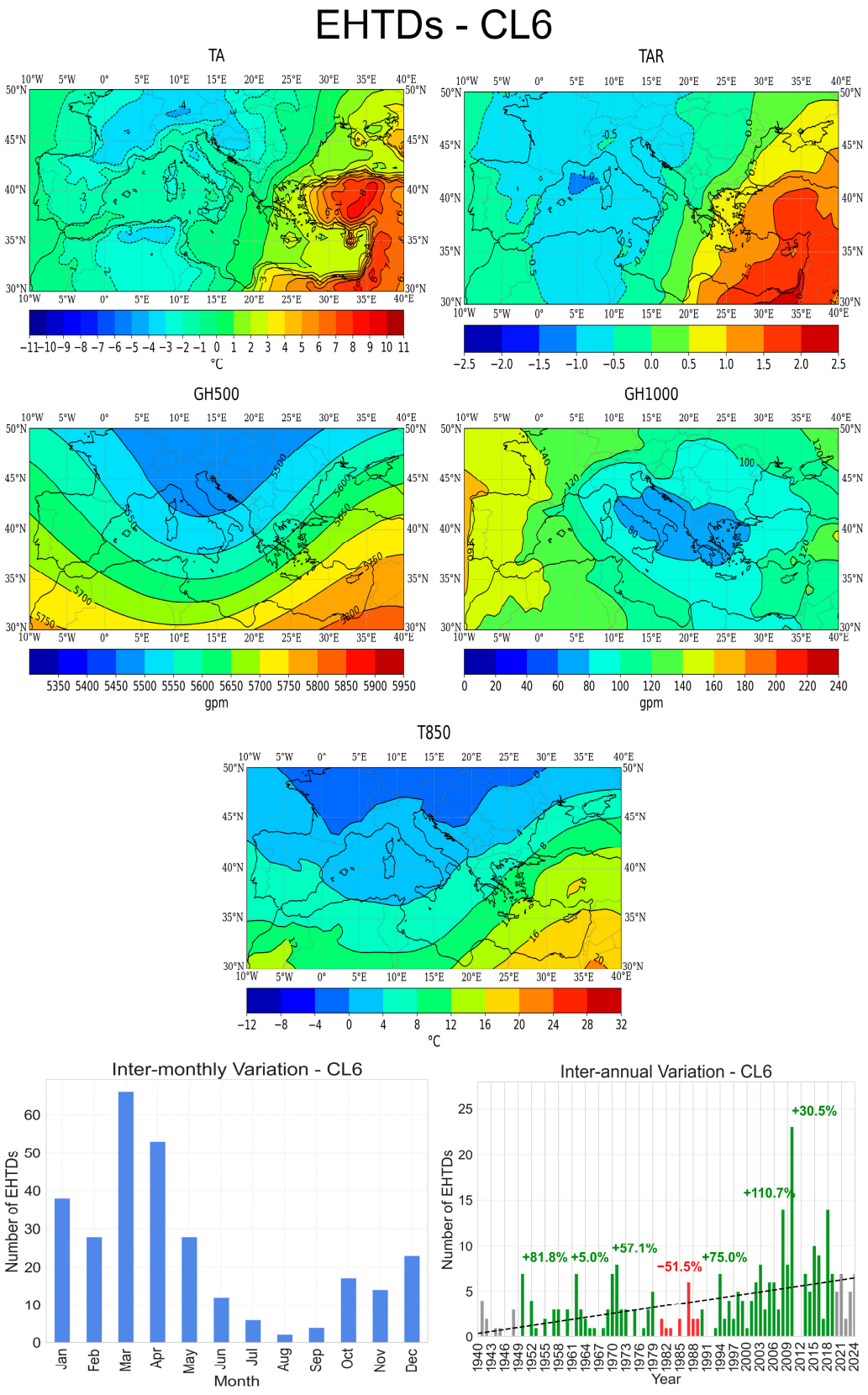

Figure 11. Same as in Figure 6, but for CL6 of EHTDs.

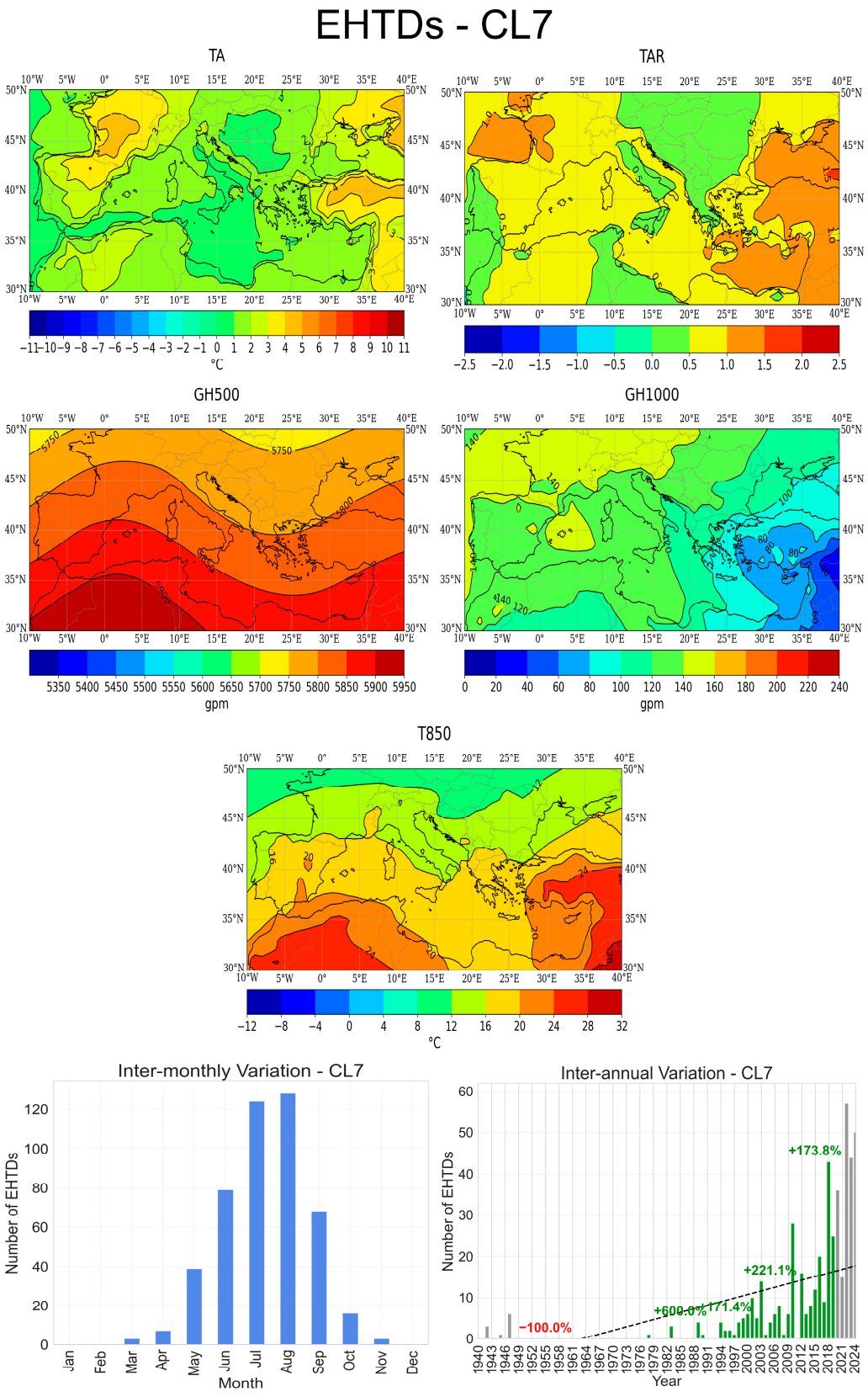

Figure 12. Same as in Figure 6, but for CL7 of EHTDs.

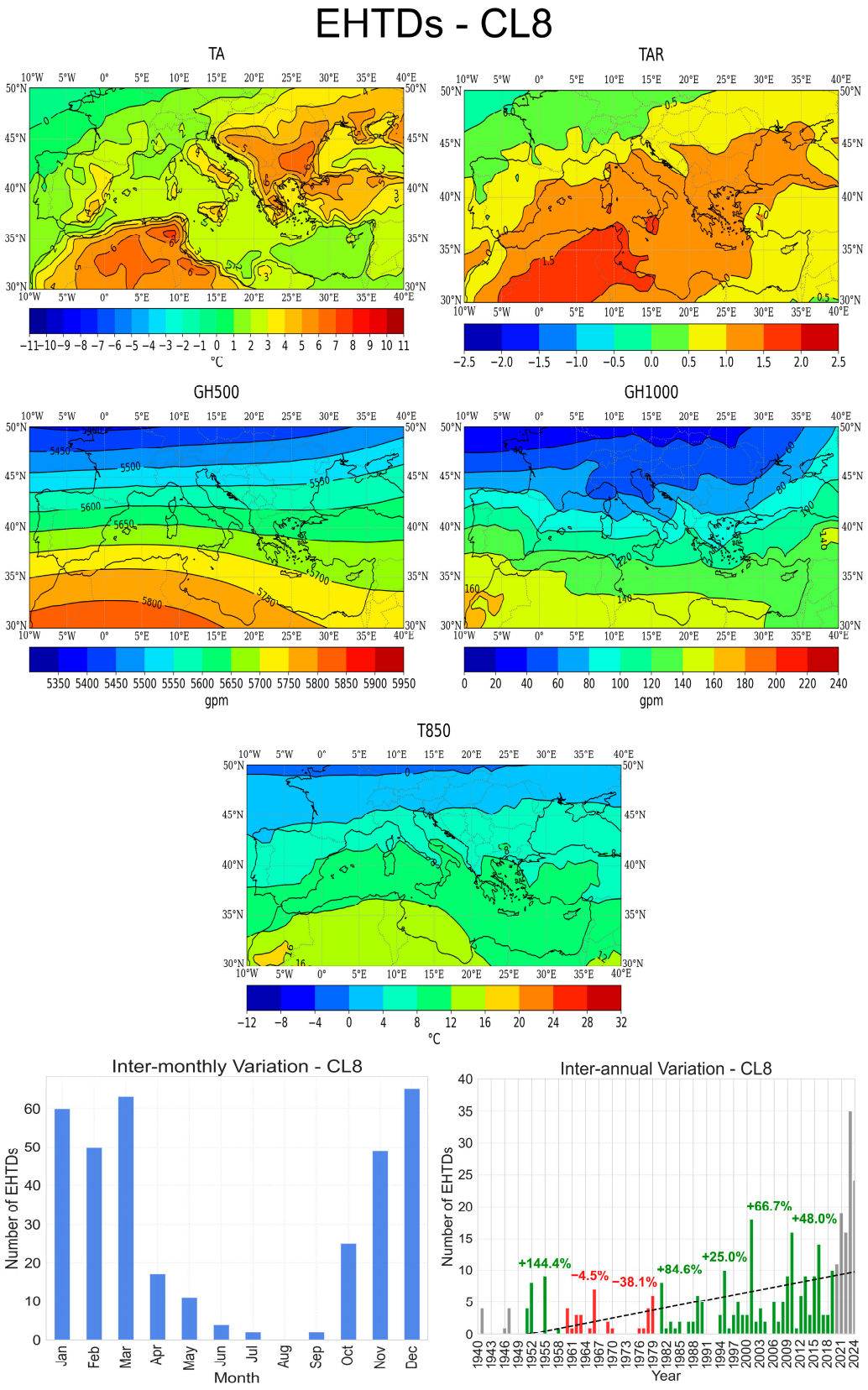

Figure 13. Same as in Figure 6, but for CL8 of EHTDs.

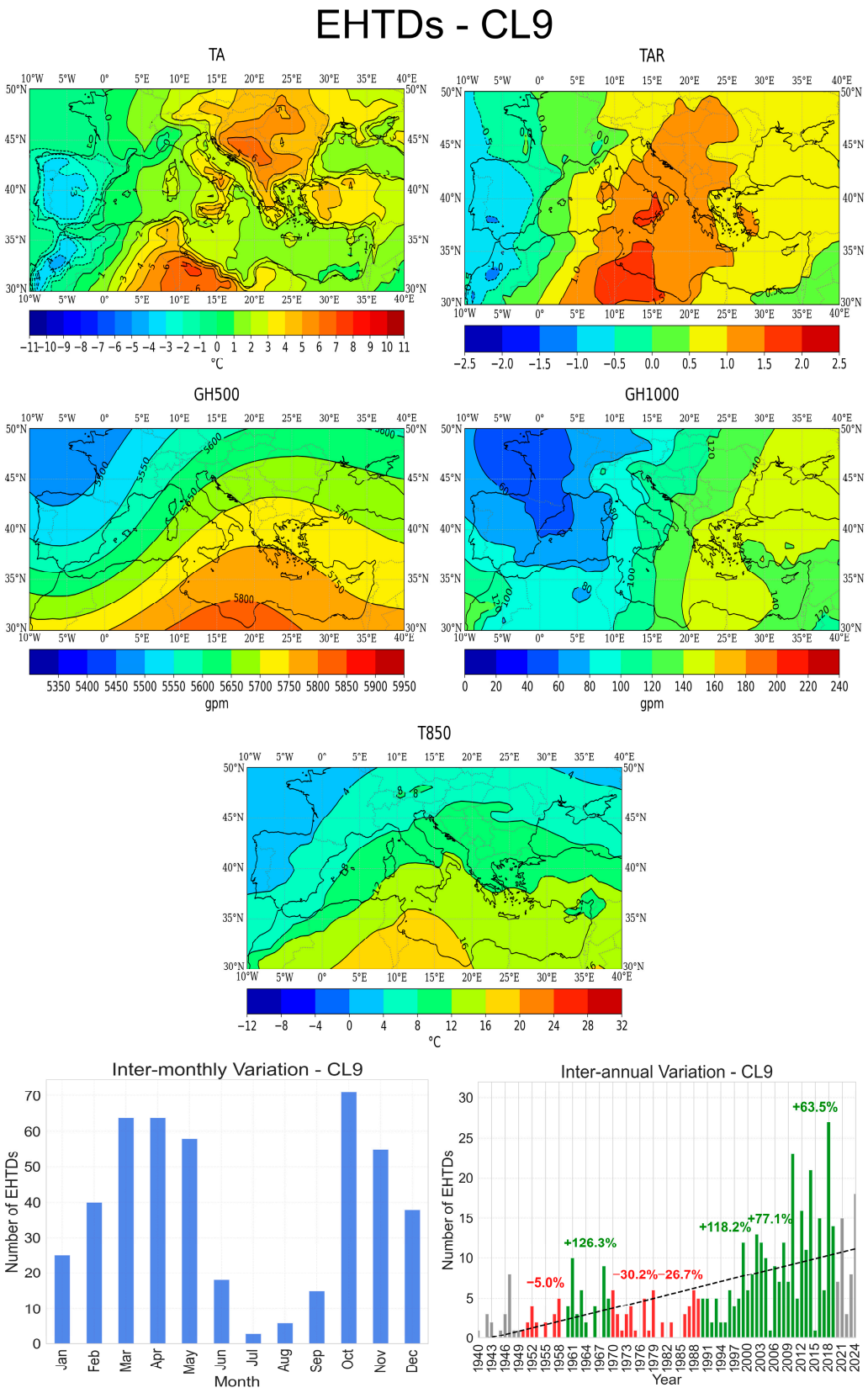

Figure 14. Same as in Figure 6, but for CL9 of EHTDs.

CL2 is a purely cold period cluster (absent in the summer months) with the highest frequencies of occurrence in December and February. The statistically significant trend revealed by the Mann–Kendal test shows that these EHTDs have become evidently more frequent, especially in the most recent decade (Figure 7). The TA and TAR values are highest

over the whole of continental Europe. Accompanying this extreme temperature pattern are a strong anticyclone at the sea level and a mid-tropospheric ridge over the central and western Mediterranean extending to the northeast. The strong ridge and the strong surface high act as blocking systems preventing cloud formation, allowing continuous solar heating and leading to sinking air which compresses and warms as it descends. These atmospheric conditions along with the positive T850 values are connected to the occurrence of prolonged extremely hot days over Europe. The aforementioned blocking high-pressure patterns are consistent with those identified by Tomczyk et al. [30], who linked similar circulation regimes to the development of prolonged heatwaves in central Europe.

CL3 is present during the whole year with a lower frequency during the winter season. The EHTDs of CL3 are also significantly more frequent in recent years (Figure 8). The TA and TAR values are positive and high over the eastern Mediterranean, including the Balkans and Middle East, whereas in the western part negative values appear. Near the surface, cyclonic conditions prevail in the eastern Mediterranean, while over the North Atlantic Ocean a strong anticyclone dominates. The combination of these two systems leads to a southern flow and warm air advection in the eastern part of the region, while in the western part a northern flow dominates leading to cold air advection, thus the negative TA and TAR values. In the troposphere, the mid-tropospheric trough and low T850 values over NW Europe are associated with the negative TA and TAR values, whereas the mid-tropospheric ridge and high T850 values over the eastern Mediterranean explain the positive TA and TAR values. Kostopoulou and Jones [31] also found a stronger summer warming in the eastern Mediterranean in comparison with the western half as well as fewer frost dates.

CL4 is purely a warm period cluster dominating mostly during the conventional summer season (June to August) and is significantly more frequent during the last two decades (Figure 9). High TA and TAR values appear over the Mediterranean Sea axis and especially over the nearby inland regions (e.g., Balkans, North Africa). The synoptic conditions of this cluster include the combination of the Azores subtropical high extension over western Europe and the SW Asian thermal low at the 1000 hPa geopotential height. This typical summer circulation causes the appearance of a northerly flow in the eastern Mediterranean Sea, known as the Etesian winds [32]. However, this combination seems relatively weak as it is not able to reduce the effect of warm advection from northern Africa and the high radiative heating of the adjacent land areas. The strong and persistent ridge at 500 hPa, the high temperatures in the lower troposphere and the extended Azores subtropical high on the surface indicate the predominance of a heat dome, where warm air is trapped and prolonged extremely warm conditions occur.

CL5 (Figure 10) mainly occurs during the warm period of the year, specifically from May to July. Also, the EHTDs of this cluster have become significantly more frequent in recent decades, as shown by the inter-annual variation. CL5 is associated with high TA and TAR values over central and western Europe. The strong anticyclonic activity near the surface leads to enhanced warming by inhibiting cloud formation and allowing continuous solar heating, while the strong ridge in the mid-troposphere results in air masses sinking, compressing and warming. These synoptic conditions favor the appearance of EHTDs over central Europe and are commonly associated with prolonged heatwaves. Similar synoptic conditions were highlighted by Tomczyk et al. [33], who associated persistent anticyclonic circulation and mid-tropospheric ridges with prolonged heatwaves in W and SW Europe.

CL6 (Figure 11) is generally a cold period cluster with the highest frequency of occurrence during March–April and EHTDs of this type appear significantly more frequently in recent years. The TA and TAR values are high in the eastern Mediterranean, including NE Africa, Greece and the Middle East. The synoptic conditions accompanying this cluster are

characterized by the prevalence of a surface depression over Greece and Italy, which leads to a S–SW flow in the eastern Mediterranean. At higher altitudes, a ridge is frequent over NE Africa where high T850 values appear. These synoptic conditions indicate warm air advection from lower latitudes resulting in extreme temperatures in the eastern Mediterranean [34]. Zhang et al. [35] also found that the frequency of warm days in the Middle East has significantly increased, exhibiting a sharp increase after 1990s which is also seen in the inter-annual variation in CL6 EHTDs.

CL7 (Figure 12) is purely a warm period cluster that prevails mainly from June to September. The intra-annual variation in the frequencies of this cluster's EHTDs shows a statistically significant positive trend, leading to an increased frequency of appearance of this type of EHTDs. Also, it seems that these EHTDs have been making their appearance during the 21st century and they were almost completely absent before. The whole Mediterranean region has high TA and TAR values, with the eastern part and western Europe exhibiting the highest values. These high values are associated with surface anticyclonic activity over NE Europe, a deep mid-tropospheric ridge originating from NW Africa and expanding north and high temperatures at the 850 hPa level over the Mediterranean Sea and coastal regions. These conditions favor the transfer of warm air masses from the southern latitudes to the Mediterranean and southern Europe.

CL8 (Figure 13) is a cold period cluster prevailing mostly from December to March and shows a very high (statistically significant) frequency of occurrence especially during the last two decades. High TA and TAR values are seen over NW Africa, in central and western Mediterranean and the Balkans. The isopleths of GH500 and GH1000 are parallel with higher values over N Africa and lower values over Europe, leading to strong westerlies over the Mediterranean. These westerlies transfer warm and humid air masses from the North Atlantic to the Mediterranean leading to the appearance of this type of EHTDs. Also, the strong ridge and high 850 hPa temperatures over NW Africa act as a heat dome, trapping warm air and preventing convection leading to extreme temperatures. This pattern supports the results of Hertig et al. [8], who also found warming trends and increasing high temperature extremes in the western Mediterranean under similar synoptic conditions.

CL9 is generally a cold period cluster which has become more frequent in recent years, especially in the last two decades. The TA and TAR values are high over the central Mediterranean and the Balkans, whereas in the western Mediterranean negative values appear (Figure 14). The combination of cyclonic activity in NW Europe and anticyclonic activity in eastern Europe results in the prevalence of a southern surface flow leading to warm air advection. Moreover, the mid-tropospheric ridge and the high T850 values over N Africa result in the entrapment of warm air leading to prolonged extremely warm days.

A summary of the results of the EHTD analysis can be seen in Table 1. Cold period EHTDs (e.g., CL1, CL2, CL6, CL8, and CL9) are typically associated with strong anticyclonic systems and mid-tropospheric ridges over Europe or North Africa. These synoptic patterns suppress cloud formation and enhance subsidence, leading to clear sky conditions and increased solar heating. In many cases, these features act as atmospheric blocking systems that trap warm air masses, favoring the development of heat domes, even during the colder months. In contrast, warm period EHTDs (e.g., CL4, CL5, and CL7) are more strongly influenced by subtropical high-pressure systems, such as the Azores High, and thermal lows, like the SW Asian thermal low. These events are often accompanied by intense radiative heating and warm air advection from North Africa. Mid-tropospheric ridges and high T850 values are common, particularly over southern and eastern Europe, and are typically associated with the occurrence of heatwaves.

Table 1. Table summarizing the results of the EHTD analysis. For each cluster, the intra-annual frequency, the main areas affected where high TA/TAR values are found and the associated synoptic patterns are shown.

CL	Intra-Annual Frequency	Main Affected Areas—High TA/TAR Values	Synoptic Pattern and Features
CL1	Cold period, max in spring	W Mediterranean (Iberian Peninsula, Algeria)	Surface anticyclone, 500 hPa ridge, high T850; heat dome
CL2	Cold period, max in winter	Continental Europe	Surface anticyclone, 500 hPa ridge; blocking system
CL3	Year-round, min in winter	E Mediterranean (Balkans, Middle East)	Depression and anticyclone combination; warm air advection
CL4	Summer	Mediterranean Sea axis, Balkans, North Africa	Strong 500 hPa ridge, high T850; heat dome
CL5	Warm period	Central and western Europe	Surface anticyclone, 500 hPa ridge; prolonged heatwaves
CL6	Cold period, max in spring	E Mediterranean (NE Africa, Greece, Middle East)	Surface depression, high T850; warm air advection
CL7	Summer	Entire Mediterranean, highest in E Mediterranean and W Europe	Surface anticyclone, 500 hPa ridge, high T850; warm air advection
CL8	Cold period	NW Africa, central and western Mediterranean, Balkans	Parallel GH500 and GH1000 isopleths; strong westerlies, heat dome
CL9	Cold period	Central Mediterranean, Balkans	Surface cyclone—anticyclone combination, 500 hPa ridge, high T850; warm air advection

3.3. ELTDs

In the case of low temperature extremes, the applied methodology led to the definition of 4872 ELTDs. Figure 15 shows the inter-monthly and inter-annual variations in the number of ELTDs. It can easily be seen that the number of ELTDs has decreased significantly (95% confidence level) during the 85-year period of 1940–2024, especially during the 21st century. Also, ELTDs occur more frequently during the cold period of the year, with the highest frequency of occurrence from December to March. Comparing the mean number of defined ELTDs during the periods 1940–1980 and 1981–2024, a decrease of 41% is found.

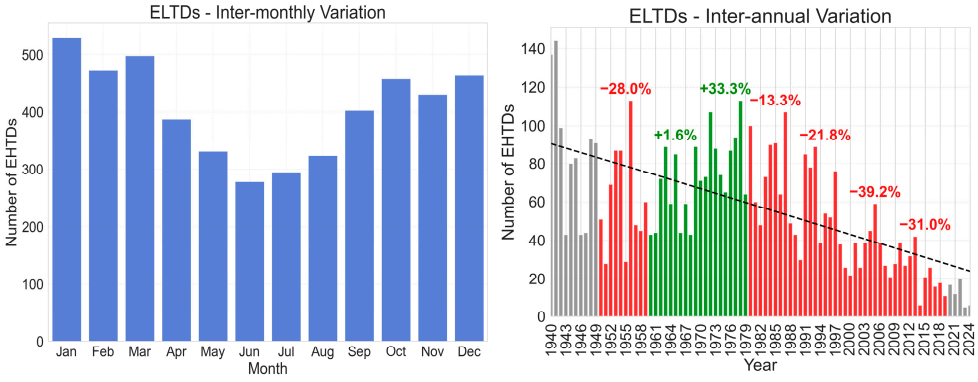

Figure 15. The inter-monthly (**left**) and the inter-annual (**right**) variations in the number of ELTDs. In the inter-annual plot, the percentages and bar colors indicate the decadal-scale changes in the mean number of ELTDs compared with the previous decade (green for an increase and red for a decrease). The gray bars represent the first decade, 1940–1949, and the incomplete decade, 2021–2024. The dashed line represents the statistically significant linear trend at 95% confidence level.

By applying FA on the time series of ELTD TAR values, eight factors are defined which correspond to 71% of the total variance. Applying FA on the GH1000, T850 and GH500 time series leads to the definition of six factors representing 85% of the total variance. Next, the 14 factors' scores are placed in a matrix (Figure 2) and by performing CA on their time series the ELTDs clusters are defined. According to the distortion test results (Figure 5b), the optimal number of clusters for classifying ELTDs appears to be either seven or nine. Both options were evaluated, but the seven clusters solution was ultimately selected. The nine cluster case produced clusters with overlapping characteristics suggesting limited added value and making them less distinct and harder to interpret. Thus, the seven cluster classification is considered the most robust and interpretable approach for capturing the key synoptic patterns associated with ELTDs. The mean spatial patterns of TA, TAR, GH500, GH1000 and T850 as well as the inter-monthly and inter-annual variations in the number of ELTDs are shown in Figures 16–22.

CL1 (Figure 16) is an all-year round cluster with lower frequencies during the conventional winter season and has become significantly less frequent in recent years. The TA and TAR values are high (negative) over the central and western Mediterranean. Near the sea level, the N–NE flow deriving from the combination of cyclonic activity over Greece–Italy and anticyclonic activity over the N Atlantic Ocean leads to cold air advection over the affected region. In the T850 field, the cold air masses originating from northern Europe are transferred into the Mediterranean. These synoptic conditions associated with extremely cold weather were also revealed by D'Errico et al. [36], who linked similar synoptic conditions to cold and snowy spells over southern Italy.

CL2 (Figure 17) is a pure cold period cluster with a high frequency of occurrence from November to March and has become less frequent in recent years. High (negative) TA and TAR values are seen in the eastern Mediterranean and the Middle East. A blocking anticyclone dominates over the entire region, leading to a cloud-free sky and enhancing radiative cooling during the night. The low T850 values favor the prevalence of extremely low surface temperatures. Zhang et al. [35], by studying extreme temperatures in the eastern Mediterranean–Middle East, found that the frequency of cold days has significantly decreased gradually from the 1970s, in agreement with the inter-annual variation in CL2 ELTDs.

CL3 is generally a warm period cluster with a higher frequency of occurrence during late summer–early autumn and has become less frequent in recent periods (Figure 18). High (negative) TA and TAR values appear over eastern Europe. The enhanced anticyclonic activity over the affected area results in air sinking, preventing cloud formation and increasing radiative cooling and thereby favoring the formation of surface inversions during the night. Also, the NE flow in the east of the anticyclone favors cold air advection. The low temperatures in the 850 hPa height confirm the advection of cold air masses. These finding coincide with the findings of Nygård et al. [37], who showed that blocking highs over northern Europe coupled with mid-tropospheric troughs often lead to the transport of cold air masses and intense nighttime radiative cooling over Europe, particularly during transitional seasons.

CL4 (Figure 19) is an all-year-round cluster with a higher frequency of occurrence during the colder months of the year. Also, this type of ELTDs occur significantly less frequently in recent decades. The TA and TAR values are high (negative) over the central and eastern Mediterranean, including Italy, Greece and the Balkans. The dominant Cyprus low combined with frequent and strong anticyclonic conditions over western Europe lead to a NE flow and cold air advection over Greece and SE Europe. The deep trough at 500 hPa and the very cold conditions in the lower troposphere indicate the invasion of cold polar air masses into the eastern Mediterranean. Tringa et al. [38] performed a climatological and synoptic

analysis of winter cold spells over the Balkan Peninsula finding that the extremely low winter temperatures in the Balkans are associated with the aforementioned synoptic conditions.

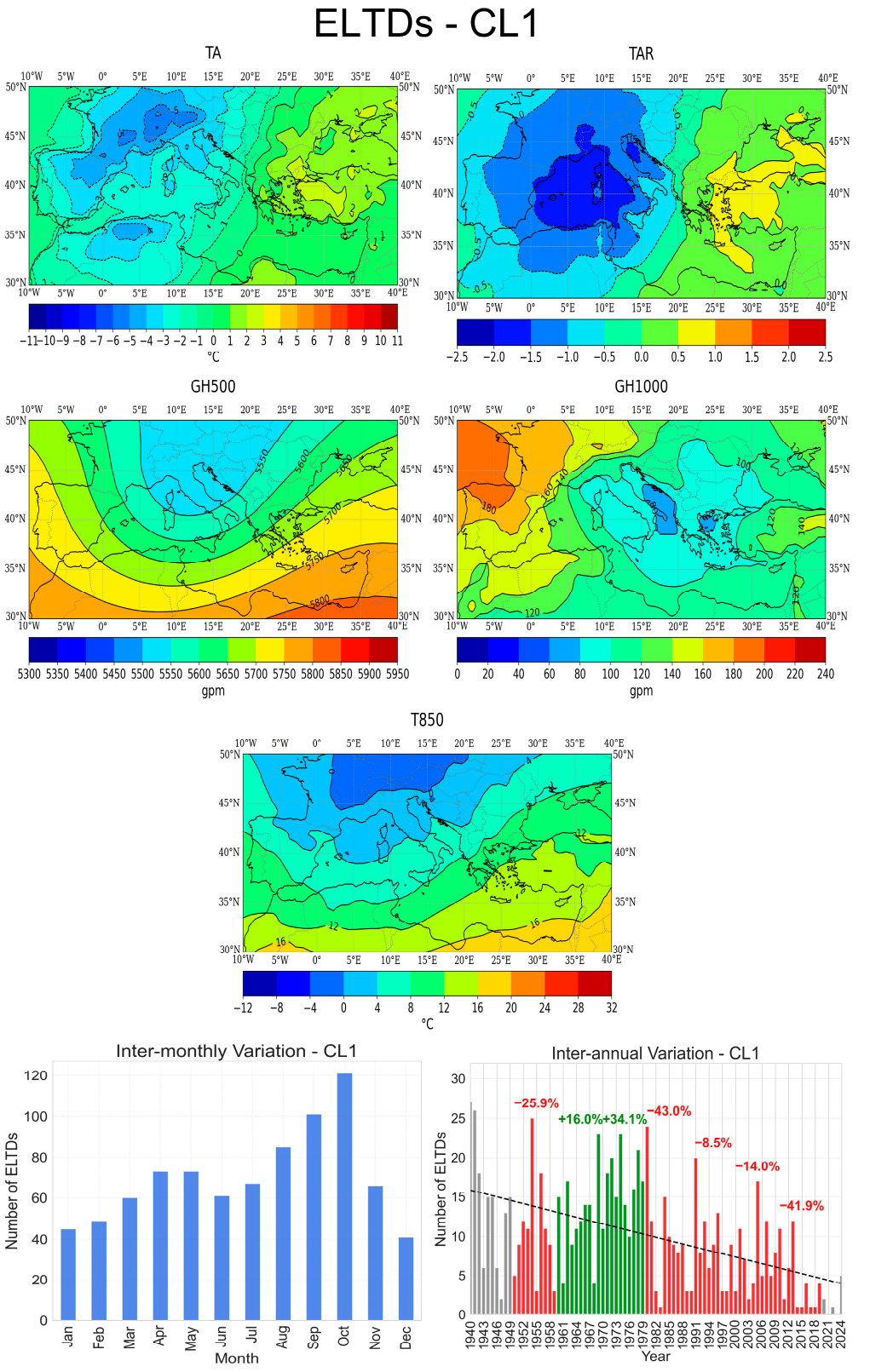

Figure 16. The TA (°C), TAR (unitless), GH500 (geopotential meters, gpm), GH1000 (geopotential meters, gpm) and T850 (°C) mean patterns and the respective inter-monthly and inter-annual variations for CL1 of ELTDs. Statistically significant trends in the inter-annual variation are shown (dashed line).

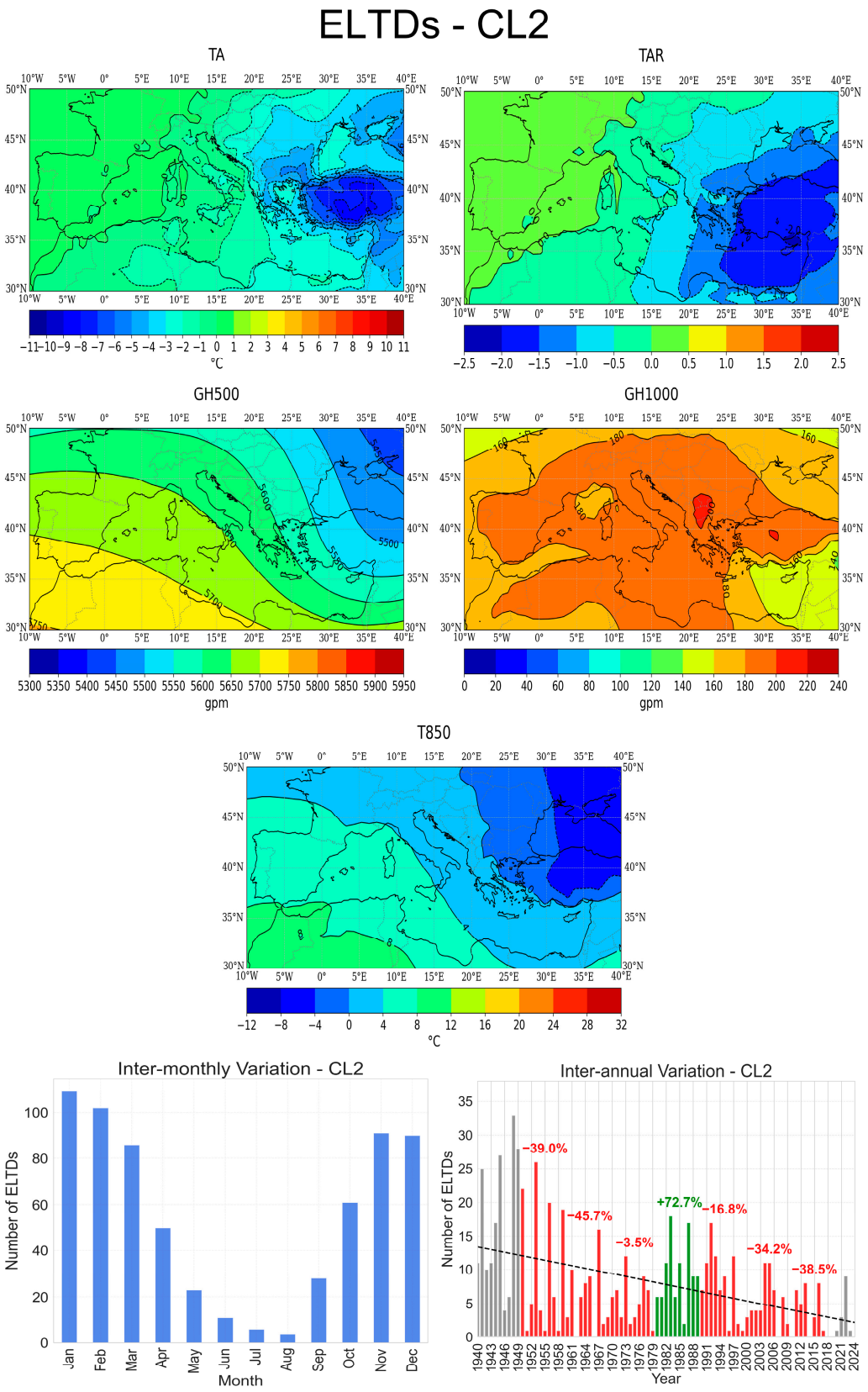

Figure 17. Same as in Figure 16, but for CL2 of ELTDs.

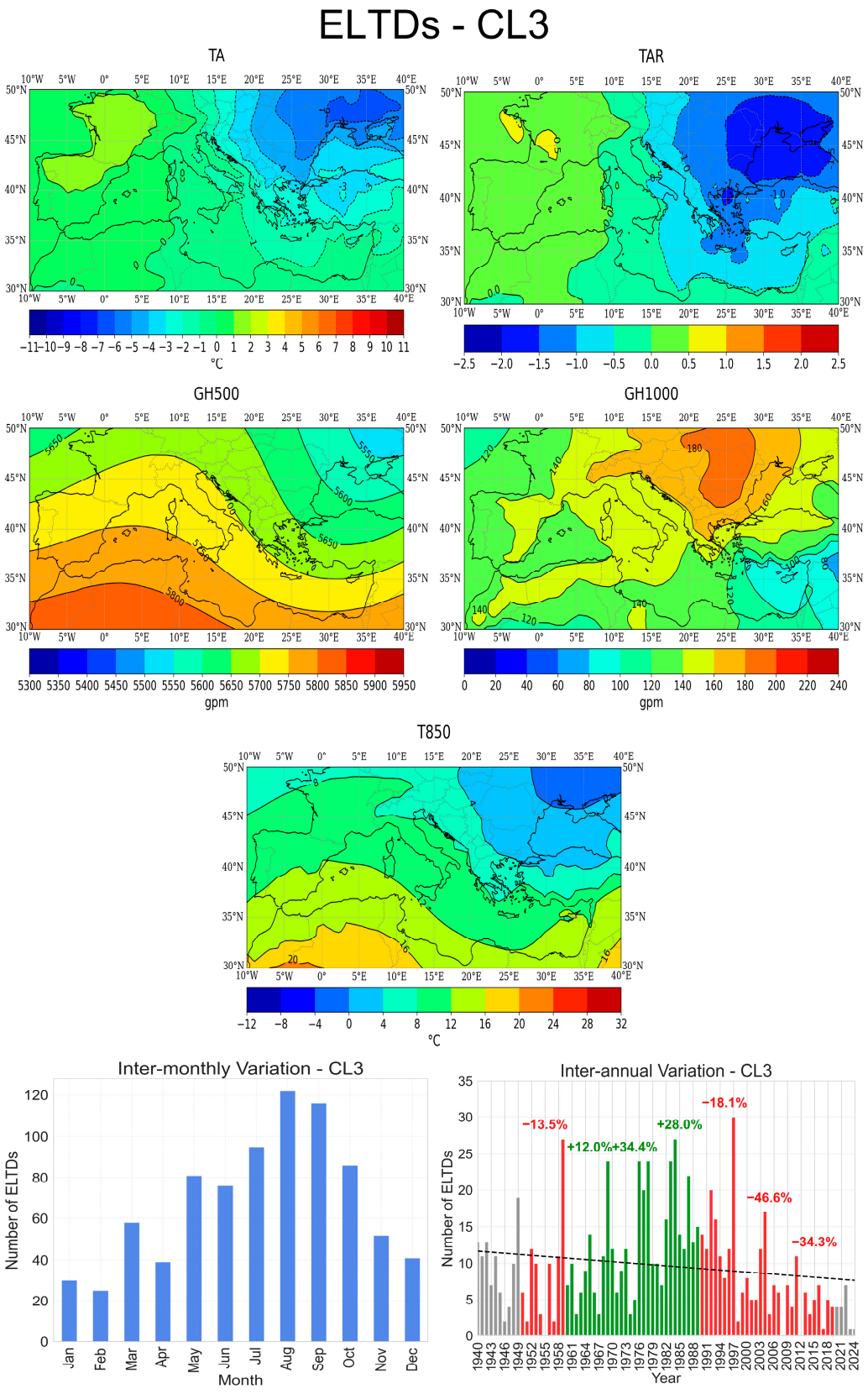

Figure 18. Same as in Figure 16, but for CL3 of ELTDs.

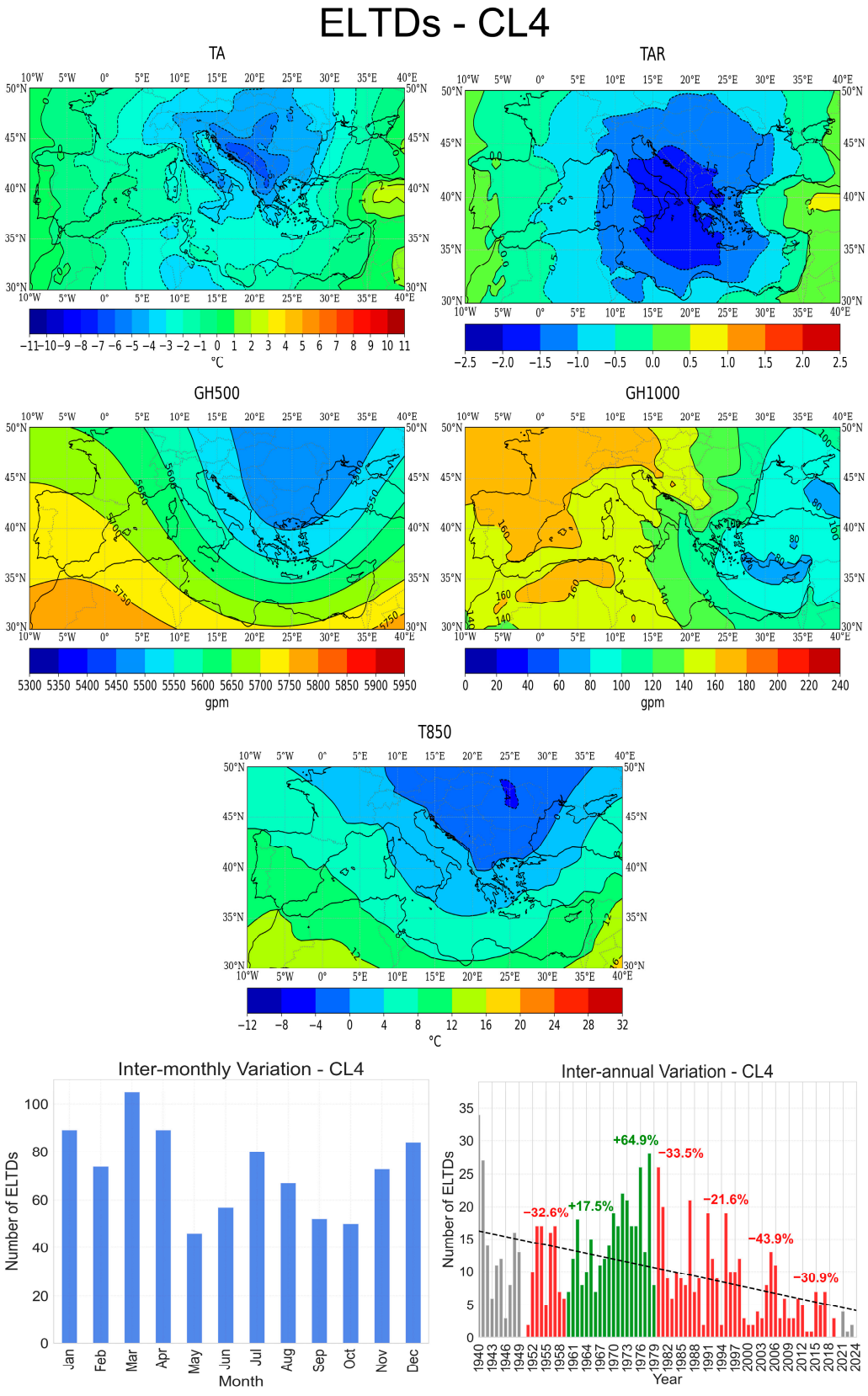

Figure 19. Same as in Figure 16, but for CL4 of ELTDs.

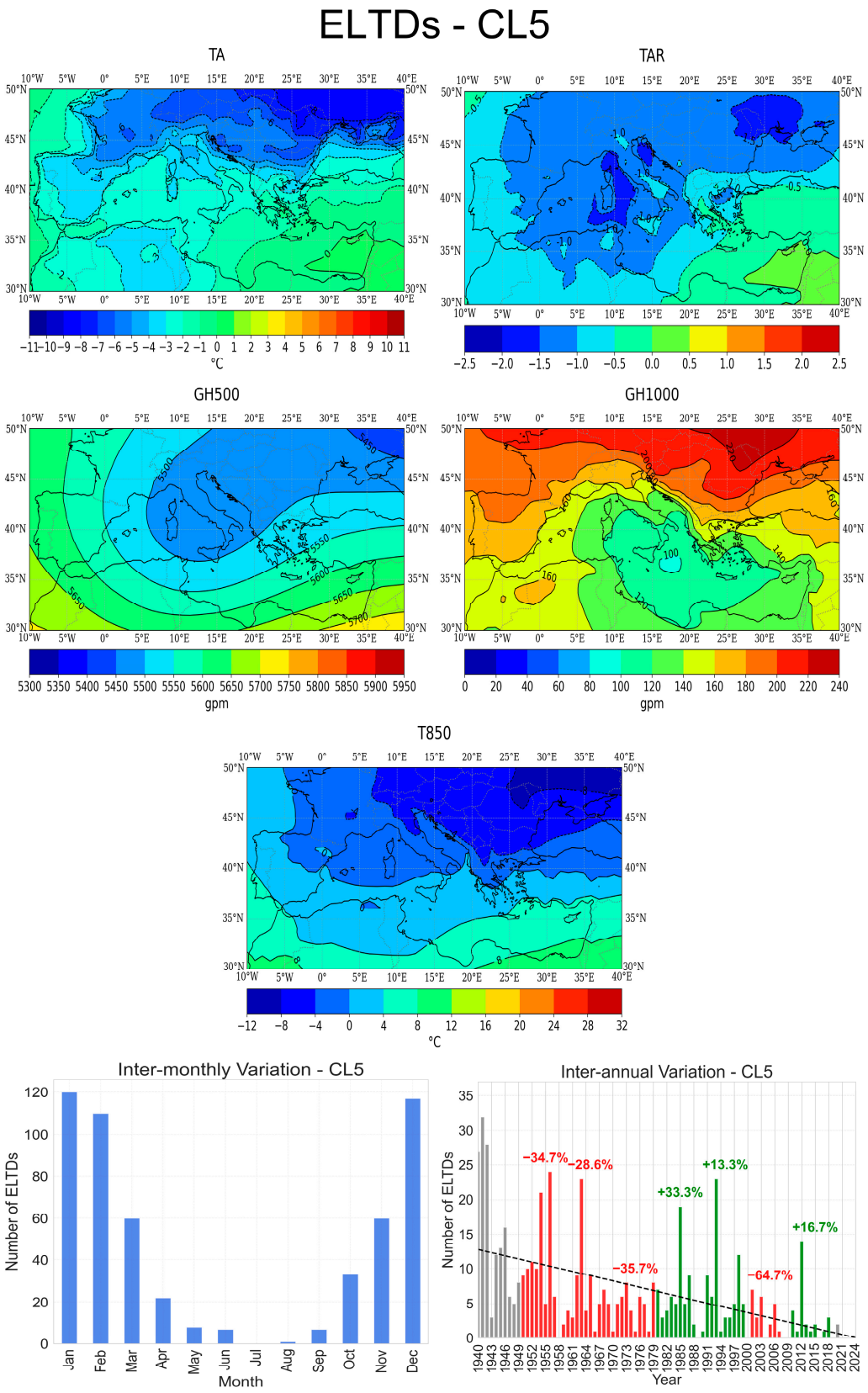

Figure 20. Same as in Figure 16, but for CL5 of ELTDs.

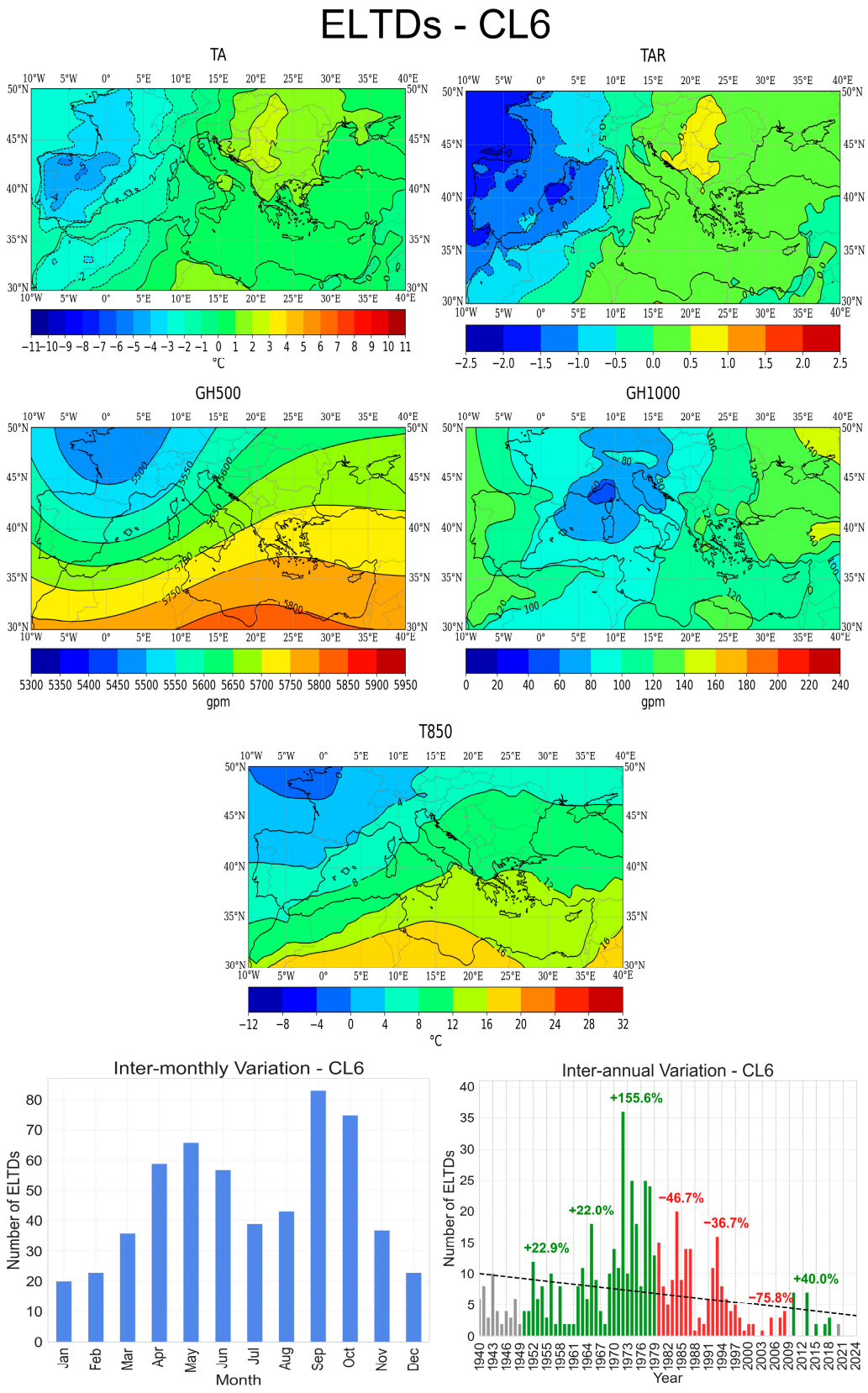

Figure 21. Same as in Figure 16, but for CL6 of ELTDs.

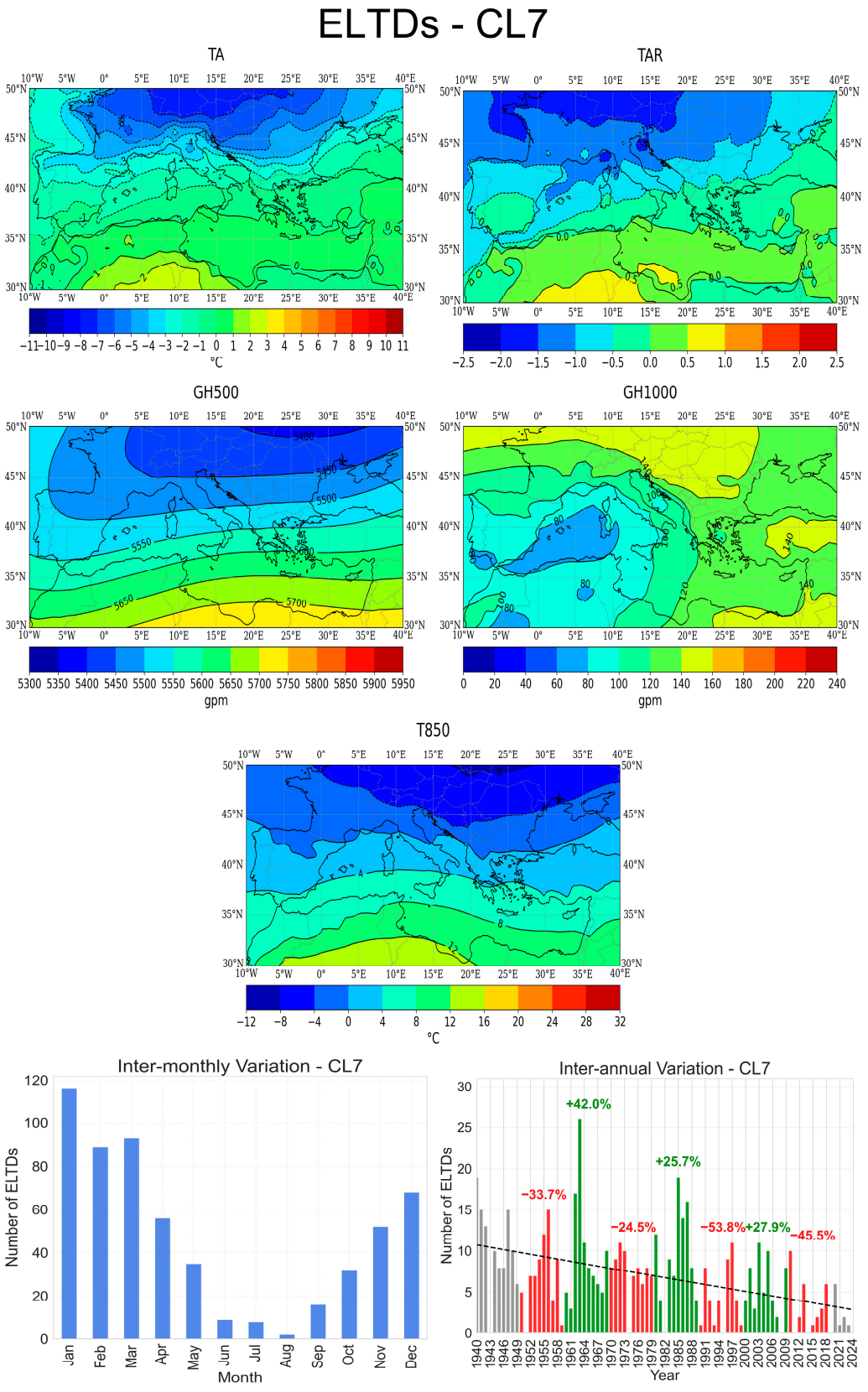

Figure 22. Same as in Figure 16, but for CL7 of ELTDs.

CL5 is a pure cold period cluster mainly dominating during the conventional winter season. Also, a statistically significant negative trend in the inter-annual frequency of occurrence of this type of ELTDs is found (Figure 20). High negative TA and TAR values appear over continental Europe and the central and western Mediterranean. The mid-tropospheric

trough and the extremely low T850 values indicate the advection of cold air masses from northern Europe. Near the sea level, a blocking anticyclone over Europe prevents convection, inhibiting cloud formation and enhancing radiative cooling. This finding aligns with the results of Trigo et al. [39], who emphasized that persistent blocking anticyclones over northern and central Europe combined with mid-tropospheric troughs often lead to severe cold spells across continental Europe due to prolonged cold air advection and radiative cooling.

CL6 ELTDs occur generally during the warm period of the year with the highest frequency in September–October (Figure 21). Also, they have become significantly less frequent after the 1980s, almost disappearing in the 21st century. The TA and TAR values are negative in the western Mediterranean. On the surface, strong and frequent cyclonic activity prevails over the central Mediterranean. In the mid-troposphere, a trough is seen over W Europe along with low T850 values and a ridge dominates in NE Africa along with high T850 values. These synoptic conditions form the TA and TAR patterns of CL6. In the western part of the surface depression, a northerly flow transports cold air masses (low 850 hPa temperatures) from northern latitudes leading to extremely low temperatures. In the eastern part of the surface depression, a southern flow dominates, transporting warmer air masses (high 850 hPa temperatures) from southern latitudes leading to warmer conditions.

Lastly, CL7 (Figure 22) is a cold period cluster with a higher frequency of occurrence from January to March. Also, it seems that the ELTDs of CL7 are less frequent in recent decades. The TA and TAR values are high (negative) over northern Europe. These values are associated with a deep trough over northern Europe along with extreme low temperatures in the lower troposphere. These conditions indicate Arctic outbreaks or polar vortex disruptions, during which the polar vortex expands, sending cold air southward with the jet stream. An association with negative NAO and AO indices together with strong Greenland blocking has also been documented [37].

A summary of the results of the ELTD analysis is shown in Table 2. Cold period ELTDs (e.g., CL2, CL4, CL5, and CL7) are frequently characterized by blocking anticyclones over Europe and the eastern Mediterranean that suppress cloud formation and intensify radiative cooling. These conditions are frequently accompanied by deep mid-tropospheric troughs and low T850 temperatures, favoring the advection of cold polar air masses. On the other hand, warm period ELTDs (e.g., CL3 and CL6) are generally associated with persistent surface cyclonic systems combined with mid-tropospheric troughs over western and central Europe, resulting in cold air advection from northern latitudes. Also, anticyclonic conditions promote enhanced radiative cooling under clear skies, leading to extremely low temperatures during the warm season. Even though both cold and warm period ELTDs are driven by cold air advection and radiative cooling processes, the mechanisms differ in intensity and pattern depending on the season of the year.

The above results refer to the extremely high/low temperatures occurring in the Mediterranean region during the last 85 years and the synoptic conditions leading to their appearance. Comparing the present findings with the results of relevant studies investigating extreme temperatures and trends over the region [8,9,11,31,35] could yield interesting insights. Kostopoulou and Jones [31] focused on the eastern Mediterranean and found stronger summer warming and fewer frost dates. These findings coincide with the results of CL3 of EHTDs (Figure 8) for the eastern Mediterranean as well as with the increased number of EHTDs during summer and the decreasing number of ELTDs in recent years. Zhang et al. [35] studied precipitation and temperature extremes using indices from data over 52 stations in the eastern Mediterranean–Middle East. They found that the frequency of warm days in the region under study has significantly increased, which

is also seen in the inter-annual variation in CL6 EHTDs, and the frequency of cold days has significantly decreased in agreement with the inter-annual variation in CL2 ELTDs. Hertig et al. [8] investigated spatial differences within the Mediterranean basin, revealing a warming trend for the western part and a cooling trend for the eastern part of the region. The warming of the western Mediterranean is also revealed in the results of CL1 and CL8 of EHTDs (Figures 6 and 13), while the cooling of the eastern Mediterranean is supported by the results of CL2 of ELTDs (Figure 17). Efthymiadis et al. [9] also found a warming of the western Mediterranean and a cooling of the eastern part of the region, which has reversed in recent years. This reversal is also revealed here as shown by the decreasing number of ELTDs in recent decades (Figure 15). Lolis et al. [11] applied a similar methodology as in the present work for the Balkan region, leading to similar results. The positive/negative statistically significant trends in the inter-annual variations in the EHTDs/ELTDs are found in both works.

Table 2. Table summarizing the results of the ELTD analysis. For each cluster, the intra-annual frequency, the main areas affected where high TA/TAR values are found and the associated synoptic patterns are shown.

CL	Intra-Annual Frequency	Main Affected Areas—High TA/TAR Values	Synoptic Pattern and Features
CL1	All-year-round	Central and western Mediterranean	Cyclone–anticyclone combination; cold air advection
CL2	Cold period	E Mediterranean and Middle East	Surface anticyclone, low T850; blocking system, radiative cooling
CL3	Warm period	E Europe	Surface anticyclone, low T850; cold advection, temperature inversions
CL4	All-year-round	Central and eastern Mediterranean (Italy, Greece, Balkans)	Cyclone–anticyclone combination, deep 500 hPa trough; cold advection, polar air mass intrusions
CL5	Cold period	Continental Europe and central/western Mediterranean	Surface blocking anticyclone, 500 hPa trough; cold air advection, radiative cooling
CL6	Warm period	W Mediterranean	Surface cyclone, 500 hPa trough, low T850; cold air advection
CL7	Cold period	N Europe	500 hPa trough, low T850; Arctic outbreaks, polar vortex disruptions

There have also been other studies investigating temperatures extremes but they have been focused on the sub-regions of the Mediterranean and for shorter time periods [40–42]. The use of an expanded domain covering the whole Mediterranean region, the application of a multivariate statistical methodology for objectively defining temperature extremes—both for the cold and warm periods of the year—and linking them with the synoptic atmospheric patterns, the investigation of the trends in temperature extremes during ongoing climate change, and the use of the recently released reanalysis data from ERA5 dating back to 1940 are the main advantages of this study.

The results of this study provide important insights that should be considered in policy and adaptation decisions for high-risk areas affected by extreme temperatures. The increasing frequency and intensity of EHTDs in vulnerable regions such as the Balkans, the Middle East and the western Mediterranean (Iberian Peninsula–NW Africa), as highlighted by clusters like CL5, CL6 and CL7, support the urgent need for targeted adaptation strategies. These findings can support early warning systems by linking specific circulation

patterns to heat extremes, enabling more accurate and timely alerts. They can also inform urban heat action plans by identifying high-risk regions where practical measures, such as establishing cooling centers, issuing public heat alerts and promoting heat-resilient urban design (e.g., increased tree cover, reflective building materials), should be prioritized to reduce exposure and strengthen public health resilience.

4. Conclusions

This study focused on investigating the characteristics and variability of temperature extremes over the Mediterranean region, aiming to better understand their spatial and temporal distribution, long-term trends and associated atmospheric circulation patterns leading to their appearance. Utilizing 85 years (1940–2024) of high-resolution ERA5 reanalysis data, the extremely high (EHTDs) and low (ELTDs) temperature days were identified and classified based on the daily 2 m temperature anomalies at 12 UTC and 06 UTC, respectively. The key findings of this work are as follows:

1. A clear intensification of temperature extremes was found. EHTDs display a significantly increased frequency, while ELTDs have significantly decreased, especially during the 21st century. These tendencies highlight a shifting of the temperature regime in the Mediterranean and are consistent with the regional warming trends linked to climate change.
2. Distinct circulation patterns were associated with each type of extreme. EHTDs typically occur under strong anticyclonic conditions, promoting blocking, solar heating and warm advection. ELTDs are associated with radiative cooling, cold advection and polar air mass intrusions. This connection between extremes and synoptic-scale atmospheric circulation conditions provides new insight into the mechanisms behind Mediterranean temperature extremes.
3. Seasonal differences were revealed. Warm period EHTDs are dominated by mid-tropospheric ridges leading to the occurrence of heatwaves, while cold period EHTDs involve atmospheric blocking systems favoring the development of heat domes. On the other hand, warm period ELTDs are characterized by persistent surface cyclonic systems resulting in cold air advection, while cold period ELTDs are associated with blocking highs favoring radiative cooling and polar air mass intrusions.
4. A high contrast in the occurrence between the extremes over land and sea was shown. This is highlighted by the effect of daytime radiative warming (peaking during summer for EHTDs) and the nighttime radiative cooling (peaking during winter for ELTDs) which are overlapping with the impact of warm and cold air advection leading to the appearance of extreme temperature days.
5. All present findings, especially the remarkable statistically significant positive/negative trends in the number of ETHDs/ELTDs, are in agreement with the recent warming of the Mediterranean climate attributed to ongoing climate change [5,43]. Compared with earlier studies, this work utilizes long-term high spatiotemporal resolution reanalysis data covering the entire Mediterranean region for clustering temperature extremes with the associated synoptic patterns, therefore filling a key knowledge gap and improving the robustness and spatial relevance of temperature extreme classifications.

Future work for further expanding our knowledge of the driving factors of extreme temperatures will be focused on the following three directions:

I. Incorporating additional parameters, such as sea surface temperatures and upper-air humidity [44,45], to better understand vertical and ocean–atmosphere interactions and their impact on temperature extremes.

II. Applying the current clustering methodology to compound events like heatwaves with drought by utilizing 2 m temperature and precipitation anomalies and involving local-scale observations and downscaled model data.

III. Investigating the connection between temperature extremes and large-scale atmospheric oscillations (NAO, AO, EA-WR) using correlation and composite analysis techniques to improve forecasting capabilities and assist in the development of early warning strategies for Mediterranean climate extremes.

Finally, these findings provide an important baseline for strengthening climate resilience and heat adaptation policies across the Mediterranean. By identifying circulation patterns linked to extreme temperature events and highlighting high-risk regions, this study offers a framework for creating targeted early warning systems, public health interventions and long-term urban planning strategies to better protect vulnerable populations in the face of climate change.

Author Contributions: Conceptualization, G.K. and C.J.L.; Formal analysis, G.K.; Methodology, G.K. and C.J.L.; Supervision, C.J.L.; Visualization, G.K.; Writing—original draft, G.K.; Writing—review and editing, G.K. and C.J.L. All authors have read and agreed to the published version of the manuscript.

Funding: This research received no external funding.

Institutional Review Board Statement: Not applicable.

Informed Consent Statement: Not applicable.

Data Availability Statement: The original data (ERA5) presented in this study are openly available in the Copernicus Climate Data Store (CDS) at https://cds.climate.copernicus.eu/datasets (accessed on 29 May 2025) implemented by the European Centre for Medium-Range Weather Forecasts (ECMWF).

Acknowledgments: The authors also thank the ECMWF, who produced the ERA5 atmospheric reanalysis dataset within the Copernicus Climate Change Service (C3S).

Conflicts of Interest: The authors declare no conflicts of interest.

References

1. *IPCC 2023: Climate Change 2023 Synthesis Report*; Contribution of Working Groups I, II and III to the Sixth Assessment Report of the Intergovernmental Panel on Climate Change; Core Writing Team, Lee, H., Romero, J., Eds.; IPCC: Geneva, Switzerland, 2023; pp. 35–115. [CrossRef]
2. Frame, D.J.; Rosier, S.M.; Noy, I.; Harrington, L.J.; Carey-Smith, T.; Sparrow, S.N.; Stone, D.A.; Dean, S.M. Climate change attribution and the economic costs of extreme weather events: A study on damages from extreme rainfall and drought. *Clim. Change* **2020**, *16*, 781–797. [CrossRef]
3. Van Garderen, L.; Feser, F.; Shepherd, T.G. A methodology for attributing the role of climate change in extreme events: A global spectrally nudged storyline. *Nat. Hazards Earth Syst.* **2021**, *21*, 171–186. [CrossRef]
4. Cramer, W.; Guiot, J.; Fader, M.; Garrabou, J.; Gattuso, J.-P.; Iglesias, A.; Lange, M.A.; Lionello, P.; Llasat, M.C.; Paz, S.; et al. Climate change and interconnected risks to sustainable development in the Mediterranean. *Nat. Clim. Change* **2018**, *8*, 972–980. [CrossRef]
5. MedECC. *Climate and Environmental Change in the Mediterranean Basin—Current Situation and Risks for the Future. First Mediterranean Assessment Report*; Cramer, W., Guiot, J., Marini, K., Eds.; Union for the Mediterranean, Plan Bleu, UNEP/MAP: Marseille, France, 2020; 632p. [CrossRef]
6. Tuel, A.; Eltahir, E.A.B. Why Is the Mediterranean a Climate Change Hot Spot? *J. Clim.* **2020**, *33*, 5829–5843. [CrossRef]
7. Xoplaki, E.; Luterbacher, J.; Paeth, H.; Dietrich, D.; Steiner, N.; Grosjean, M.; Wanner, H. European spring and autumn temperature variability and change of extremes over the last half millennium. *Geophys. Res. Lett.* **2005**, *32*, L15713. [CrossRef]
8. Hertig, E.; Seubert, S.; Jacobeit, J. Temperature extremes in the Mediterranean area: Trends in the past and assessments for the future. *Nat. Hazards Earth Syst. Sci.* **2010**, *10*, 2039–2050. [CrossRef]
9. Efthymiadis, D.; Goodess, C.M.; Jones, P.D. Trends in Mediterranean gridded temperature extremes and large-scale circulation influences. *Nat. Hazards Earth Syst. Sci.* **2011**, *11*, 2199–2214. [CrossRef]

10. Lionello, P.; Scarascia, L. The relation of climate extremes with global warming in the Mediterranean region and its north versus south contrast. *Reg. Environ. Change* **2020**, *20*, 31. [CrossRef]
11. Lolis, C.J.; Kotsias, G.; Farmakidis, D. A 40-year climatology of air temperature extremes in the southern Balkans based on the ERA5 database. *Theor. Appl. Climatol.* **2022**, *149*, 355–377. [CrossRef]
12. Zittis, G.; Almazroui, M.; Alpert, P.; Ciais, P.; Cramer, W.; Dahdal, Y.; Fnais, M.; Francis, D.; Hadjinicolaou, P.; Howari, F.; et al. Climate Change and Weather Extremes in the Eastern Mediterranean and Middle East. *Rev. Geophys.* **2022**, *60*, e2021RG000762. [CrossRef]
13. Bağçaci, S.Ç.; Yucel, I.; Duzenli, E.; Yilmaz, M.T. Intercomparison of the expected change in the temperature and the precipitation retrieved from CMIP6 and CMIP5 climate projections: A Mediterranean hot spot case, Turkey. *Atmos. Res.* **2021**, *256*, 105576. [CrossRef]
14. Lorenzo, N.; Díaz-Poso, A.; Royé, D. Heatwave intensity on the Iberian Peninsula: Future climate projections. *Atmos. Res.* **2021**, *258*, 105655. [CrossRef]
15. Ntoumos, A.; Hadjinicolaou, P.; Zittis, G.; Lelieveld, J. Updated Assessment of Temperature Extremes over the Middle East–North Africa (MENA) Region from Observational and CMIP5 Data. *Atmosphere* **2020**, *11*, 813. [CrossRef]
16. Papadopoulos, G.; Keppas, S.C.; Parliari, D.; Kontos, S.; Papadogiannaki, S.; Melas, D. Future Projections of Heat Waves and Associated Mortality Risk in a Coastal Mediterranean City. *Sustainability* **2024**, *16*, 1072. [CrossRef]
17. Hersbach, H.; Bell, B.; Berrisford, P.; Hiraharaet, S.; Horányi, A.; Muñoz-Sabater, J.; Nicolas, J.; Peubey, C.; Radu, R.; Schepers, D.; et al. The ERA5 global reanalysis. *Q. J. R. Meteorol. Soc.* **2020**, *146*, 1999–2049. [CrossRef]
18. Korhonen, N.; Hyvärinen, O.; Kollanus, V.; Lanki, T.; Jokisalo, J.; Kosonen, R.; Richardson, D.S.; Jylhä, K. The probabilistic skill of extended-range heat wave forecasts over Europe. *Nat. Hazards Earth Syst. Sci.* **2025**, *25*, 1865–1879. [CrossRef]
19. Jiang, N.; Cheung, K.; Luo, K.; Beggs, P.J.; Zhou, W. On two different objective procedures for classifying synoptic weather types over east Australia. *Int. J. Climatol.* **2012**, *32*, 1475–1494. [CrossRef]
20. Kotsias, G.; Lolis, C.J.; Hatzianastassiou, N.; Lionello, P.; Bartzokas, A. A comparison of different approaches for the definition of seasons in the Mediterranean region. *Int. J. Climatol.* **2021**, *42*, 1954–1974. [CrossRef]
21. Lin, S.; Wei, K.; Lei, Q.; Shao, F.; Wang, Q.; Deng, M.; Su, L. Identification and prediction of climate factors based on factor analysis and a grey prediction model in China. *Environ. Monit. Assess.* **2023**, *195*, 751. [CrossRef]
22. Jolliffe, I.T. *Principal Component Analysis*; Springer: New York, NY, USA, 1986.
23. Richman, M.B. Rotation of principal components. *Int. J. Climatol.* **1986**, *6*, 293–335. [CrossRef]
24. Wong, M.A.; Hartigan, J.A. Algorithm AS 136: A k-means clustering algorithm. *J. R. Stat. Soc. Ser. C Appl. Stat.* **1979**, *28*, 100–108.
25. Sharma, S. *Applied Multivariate Techniques*; Wiley: New York, NY, USA, 1995.
26. Sugar, A.C.; James, M.G. Finding the number of clusters in a dataset: An information–theoretic approach. *J. Am. Stat. Assoc.* **2003**, *98*, 750–763. [CrossRef]
27. Kendall, M. *Multivariate Analysis*; Charles Griffin: London, UK, 1975; p. 210.
28. Di Bernardino, A.; Casadio, S.; Iannarelli, A.M.; Siani, A.M. Temperature Trends and Influence of the Base Period Selection on Climate Indices in the Mediterranean Region over the Period 1961–2020. *Int. J. Climatol.* **2024**, *44*, 5969–5985. [CrossRef]
29. Zhang, X.; Zhou, T.; Zhang, W.; Zhu, C.; Yang, F.; Li, C.; Gao, J.; Sun, Y. Increased impact of heat domes on 2021-like heat extremes in North America under global warming. *Nat. Commun.* **2023**, *14*, 1690. [CrossRef]
30. Tomczyk, A.M.; Bednorz, E. Heat waves in Central Europe and their circulation conditions. *Int. J. Climatol.* **2016**, *36*, 770–782. [CrossRef]
31. Kostopoulou, E.; Jones, P. Assessment of climate extremes in the Eastern Mediterranean. *Meteorol. Atmos. Phys.* **2005**, *89*, 69–85. [CrossRef]
32. Tyrlis, E.; Lelieveld, J. Climatology and dynamics of the summer Etesian winds over the eastern Mediterranean. *J. Atmos. Sci.* **2013**, *70*, 3374–3396. [CrossRef]
33. Tomczyk, A.M.; Półrolniczak, M.; Bednorz, E. Circulation conditions' effect on the occurrence of heat waves in Western and Southwestern Europe. *Atmosphere* **2017**, *8*, 31. [CrossRef]
34. Hochman, A.; Marra, F.; Messori, G.; Pinto, J.G.; Raveh-Rubin, S.; Yosef, Y.; Zittis, G. Extreme weather and societal impacts in the eastern Mediterranean. *Earth Syst. Dynam.* **2022**, *13*, 749–777. [CrossRef]
35. Zhang, X.; Aguilar, E.; Sensoy, S.; Melkonyan, H.; Tagiyeva, U.; Ahmed, N.; Kutaladze, N.; Rahimzadeh, F.; Taghipour, F.; Hantosh, T.H.; et al. Trends in Middle East climate extreme indices from 1950 to 2003. *J. Geophys. Res.* **2005**, *110*, D22104. [CrossRef]
36. D'Errico, M.; Pons, F.; Yiou, P.; Tao, S.; Nardini, C.; Lunkeit, F.; Faranda, D. Present and future synoptic circulation patterns associated with cold and snowy spells over Italy. *Earth Syst. Dynam.* **2022**, *13*, 961–992. [CrossRef]
37. Nygård, T.; Papritz, L.; Naakka, T.; Vihma, T. Cold wintertime air masses over Europe: Where do they come from and how do they form? *Weather Clim. Dynam.* **2023**, *4*, 943–961. [CrossRef]
38. Tringa, E.; Tolika, K.; Anagnostopoulou, C.; Kostopoulou, E. A Climatological and Synoptic Analysis of Winter Cold Spells over the Balkan Peninsula. *Atmosphere* **2022**, *13*, 1851. [CrossRef]

39. Trigo, R.M.; Trigo, I.F.; DaCamara, C.C.; Osborn, T.J. Climate impact of the European winter blocking episodes from the NCEP/NCAR Reanalyses. *Clim. Dyn.* **2004**, *23*, 17–28. [CrossRef]
40. Brunet, M.; Jones, P.D.; Sigró, J.; Saladié, O.; Aguilar, E.; Moberg, A.; Della-Marta, P.M.; Lister, D.; Walther, A.; López, D. Temporal and spatial temperature variability and change over Spain during 1850–2005. *J. Geophys. Res.* **2007**, *112*, D12117. [CrossRef]
41. Bartolini, G.; Morabito, M.; Crisci, A.; Grifoni, D.; Torrigiani, T.; Petralli, M.; Maracchi, G.; Orlandini, S. Recent trends in Tuscany (Italy) summer temperature and indices of extremes. *Int. J. Climatol.* **2008**, *28*, 1751–1760. [CrossRef]
42. Kuglitsch, F.G.; Toreti, A.; Xoplaki, E.; Della-Marta, P.M.; Zerefos, C.; Türkes¸, M.; Luterbacher, J. Heat wave changes in the eastern Mediterranean since 1960. *Geophys. Res. Lett.* **2010**, *37*, L0482. [CrossRef]
43. Knobler, S.; Rilov, G.; Garfinkel, C.I.; Liberzon, D. Climate change impacts in Eastern Mediterranean Sea: Trends and extremes. *Water Waves* **2025**. [CrossRef]
44. Zveryaev, I.I.; Arkhipkin, A.V. Structure of climatic variability of the Mediterranean sea surface temperature, Part, I. Standard deviations and linear trends. *Russ. Meteorol. Hydrol.* **2008**, *33*, 377–382. [CrossRef]
45. Zveryaev, I.I.; Arkhipkin, A.V. Structure of climatic variability of the Mediterranean sea surface temperature, Part II. Principal modes of variability. *Russ. Meteorol. Hydrol.* **2008**, *33*, 446–452. [CrossRef]